Published in final edited form as:
Brain Struct Funct. 2009 September ; 213(4-5): 375–393. doi:10.1007/s00429-009-0214-8.

Distribution of D_1 and D_5 dopamine receptors in the primate and rat basolateral amygdale

E. Chris Muly[1,2,3,4], **Murat Senyuz**[3], **Zafar U. Khan**[5], **Jidong Guo**[2,4], **Rimi Hazra**[2,4], and **Donald G. Rainnie**[2,4]

[1]Atlanta Department of Veterans Affairs Medical Center, Decatur, GA

[2]Department of Psychiatry and Behavioral Sciences, Emory University, Atlanta, GA

[3]Division of Neuroscience, Yerkes National Primate Research Center, Atlanta, GA

[4]Center for Behavioral Neuroscience, Yerkes National Primate Research Center, Atlanta, GA

[5]Lab. Neurobiology, CIMES, Faculty of Medicine, University of Malaga, Malaga, Spain

Abstract

Dopamine, acting at the D1 family receptors (D1R) is critical for the functioning of the amygdala, including fear conditioning and cue-induced reinstatement of drug self administration. However, little is known about the different contributions of the two D1R subtypes, D_1 and D_5. W identified D_1-immunoreactive patches in the primate that appear similar to the intercalated cell masses reported in the rodent; however, both receptors were present across the subdivisions of the primate amygdala including the basolateral amygdala (BLA). Using immunoelectron microscopy, we established that both receptors have widespread distributions in BLA. The D1R subtypes colocalize in dendritic spines and terminals, with D_1 predominant in spines and D_5 in terminals. Single cell PCR confirmed that individual BLA projection neurons express both D_1 and D_5 mRNA. The responses of primate BLA neurons to dopamine and D1R drugs were studied using *in vitro* slices. We found that responses were similar to those previously reported in rat BLA neurons and included a mixture of postsynaptic and presynaptic actions. Given this we investigated the distribution of D1R in the rat BLA and found that there were similarities between the species, such as more prominent D_5 localization to presynaptic structures. The higher affinity of D_5 for dopamine suggests that presynaptic actions may predominate in the BLA at low levels of dopamine, while postsynaptic effects increase and dominate as dopaminergic drive increases. The results presented here suggest a complex action of dopamine on BLA circuitry that may evolve with different degrees of dopaminergic stimulation.

Keywords

ultrastructure; electrophysiology; non-human primate; rodent; RT-PCR; macaque; dopamine; receptor; D1; D5; electron microscopy

Dopaminergic neurotransmission at D1 family receptors (D1R) is critical for the functioning of the amygdala. Hence, D1R activation in the basolateral amygdala (BLA) is necessary for the formation of cross-modal associations between conditioned stimuli and unconditioned stimuli in fear conditioning paradigms (Lamont and Kokkinidis, 1998; Nader and LeDoux, 1999; Guarraci et al., 1999; Greba and Kokkinidis, 2000; Macedo et al., 2007), and

Corresponding Author: E. Chris Muly, Yerkes National Primate Research Center, 954 Gatewood Rd. NE, Atlanta, GA 30322, telephone (404)727-9603, facsimile (404)727-3278, emuly@emory.edu.

injections of D1R antagonists into the amygdala have anxiolytic effects (de la Mora et al., 2005). Moreover, D1R activation in the BLA is also essential for cue-induced reinstatement of drug self administration (Ciccocioppo et al., 2001; See et al., 2001; See et al., 2003; Berglind et al., 2006).

Recently, the cellular effects of dopamine activation of D1R in the amygdala have begun to be explored. D1R activation has been shown to increase the excitability of projection neurons (Kroner et al., 2005; Pickel et al., 2006; Yamamoto et al., 2007), and inhibitory interneurons in the basolateral complex (Loretan et al., 2004; Kroner et al., 2005), although GABAergic neurons in the intercalated cell groups are inhibited by D1R activation (Marowsky et al., 2005). Furthermore, activation of D1R attenuates excitatory glutamatergic input onto BLA projection neurons from the prefrontal cortex (Rosenkranz and Grace, 2002), perhaps via suppressing NMDA receptor mediated currents associated with these inputs (Pickel et al., 2006). Clearly D1R activation plays a complex role in regulating the input-output relationship of the BLA.

Despite the established importance of D1R in the normal function of the BLA, the relationship of D1R to BLA circuitry is unclear. Critically, the D1 family of dopamine receptors consists of two separate receptors, the D_1 and D_5 receptors (Civelli et al., 1993; Gingrich and Caron, 1993). While available pharmacological tools do not differentiate between these receptors, a growing body of evidence points to important functional differences (Sunahara et al., 1991; Tiberi et al., 1991; Hersi et al., 2000; Liu et al., 2000; Lee et al., 2002; Centonze et al., 2003; Laplante et al., 2004).

Consistent with results from D1R binding (Scibilia et al., 1992), in the rat, low levels of D_1 mRNA have been reported in the BLA (Mansour et al., 1991) with higher levels of D_1 mRNA (Maltais et al., 2000) and immunolabeling (Fuxe et al., 2003; Jacobsen et al., 2006) seen in the intercalated cell groups of the amygdala. Two studies have examined the subcellular distribution of D_1 in the amygdala but with contrasting findings. In the first study of the BLA, D_1-immunoreactivity (-IR) was reported mainly in cell bodies and dendrites, with spines and axon terminals more rarely seen (Pickel et al., 2006). The second study in the BLA and intercalated cell groups reported that D_1-IR was most commonly seen in dendritic spines, with dendritic shafts, axonal elements and glia less commonly seen (Pinto and Sesack, 2008). Levels of D_5 in the amygdala have not been examined directly, but low levels were inferred from studies of D1R binding in D_1-knockout mice (Montague et al., 2001). To date, no study has examined the subcellular distribution of D_5 receptors in the BLA.

The goal of this study was to establish the pattern of distribution of D_1 receptors in the BLA with a larger, quantitative analysis and compare that directly with the D_5 receptor distribution. We focused our work on macaque monkey tissue to better relate to our previous work on D_1 and D_5 in monkey prefrontal cortex. In addition, we used in vitro slice electrophysiology to examine some of the actions of D1R stimulation and examine whether previous findings in rat amygdala could be replicated in a non-human primate model. Finally, we quantified the distribution of D_1 and D_5 in rat BLA to compare to our monkey findings.

Materials and Methods

Antisera

Two antibodies were used in this study. The rat anti- D_1 antiserum (Sigma-Aldrich, St. Louis, MO, #D187) was prepared against a 97 amino acid synthetic peptide corresponding to the C-terminus of the human D_1 receptor. The antiserum stains 2 major bands at 40–45

and 65–75 kD (Hersch et al., 1995), and all staining at the light and electron microscopic levels was abolished when the antiserum was preincubated with 0.5 mg/ml of D_1-GST fusion protein (Smiley et al., 1994). The D_5 antiserum was a rabbit polyclonal antiserum raised against residues 428–438 of the D_5 receptor. This sequence is common to both rat and human D_5 receptors. This antiserum reacts to D_5-expressing recombinant Sf9 cells but not Sf9 cells expressing D_1, D_2, D_3 or D_4 (Khan et al., 2000). Western blot in macaque PFC, striatum and hippocampus labeled a single band with a molecular weight of approximately 53–54 kD (Bordelon-Glausier et al., 2008), in line with the predicted molecular weight of the D_5 receptor of approximately 53 kD (Sunahara et al., 1991; Tiberi et al., 1991). Immunohistochemical staining of macaque brain was abolished when the antiserum was pre-incubated with the cognate peptide (Bordelon-Glausier et al., 2008).

Animals and preparation of tissue for immunohistochemistry

Tissue from eight *Macaca mulatta* monkeys and 5 adult male rats were used for this study. The care of the animals and all anesthesia and sacrifice procedures in this study were performed according to the National Institutes for Health Guide for the Care and Use of Laboratory Animals and were approved by the Institutional Animal Care and Use Committee of Emory University. The animals were sacrificed with an overdose of pentobarbital (100mg/kg) and then perfused with a flush of Tyrode's solution. The flush was followed by 4 liters of fixative solution of 4% paraformaldehyde/0.2% glutaraldehyde/0–0.2% picric acid in phosphate buffer (0.1M, pH 7.4; PB). The brain was blocked and post-fixed in 4% paraformaldehyde for 2–12 hours. Coronal, 50 μm thick vibratome sections of the medial temporal lobe were cut and stored frozen at −80°C in 15% sucrose until immunohistochemical experiments were performed.

Single-label immunohistochemistry

Single-label immunoperoxidase labeling was performed using rat anti-D_1 at a 1:500 dilution or rabbit anti-D_5 antisera at 1:500. The single-label immunoperoxidase labeling for D_1 and D_5 was performed as described previously (Muly et al., 2003). Briefly, sections were thawed, incubated in blocking serum (3% normal goat serum, 1% bovine serum albumin, 0.1% glycine, 0.1% lysine) in 0.01 M phosphate buffered saline, (PBS; pH 7.4) for 1 hour and then placed in primary antiserum diluted in blocking serum. After 36 hours at 4°C, the sections were rinsed and placed in a 1:200 dilution of biotinylated donkey anti-rat IgG (Jackson Immuno Research, West Grove, PA) for D_1 or goat anti-rabbit IgG (Vector, Burlingame, CA) for D_5 for 1 hour at room temperature. The sections were then rinsed, placed in avidin-biotinylated peroxidase complex (ABC) (ABC Elite, Vector, Burlingame, CA) for 1 hour at room temperature, and then processed to reveal peroxidase using 3,3'-diaminobenzidine (DAB) as the chromagen. Sections were then post-fixed in osmium tetroxide, stained *en bloc* with uranyl acetate, dehydrated, and embedded in Durcupan resin (Electron Microscopy Sciences, Fort Washington, PA). Selected regions were mounted on blocks, and ultrathin sections were collected onto pioloform-coated slot grids and counterstained with lead citrate. Control sections processed as above except for the omission of the primary immunoreagent, did not contain DAB label upon electron microscopic examination.

Double-label immunogold/DAB immunohistochemistry

To examine the possibility of co-localization of the two D1R subtypes, we performed double-label immunogold/DAB experiments. In one condition D_1 was labeled with immunogold, and D_5 was labeled with DAB. In a second condition the labels were reversed. Amygdala tissue sections were thawed and rinsed in PBS. They were incubated in blocking serum (3% normal goat serum, 1% bovine serum albumin, 0.1% glycine, 0.1% lysine and 0.5% fish gelatin) in PBS for one hour and then placed in the primary antiserum diluted at

the same concentrations as the single label experiments overnight at 4°C. The sections were removed from the primary antiserum, rinsed in PBS and placed in secondary antiserum (1nm gold conjugated goat anti-rat, used at 1:100, Nanoprobes, Yaphank, NY and biotinylated goat anti-rabbit, used at 1:200, Jackson Immuno Research, West Grove, PA; 1nm gold conjugated goat anti-rabbit, used at 1:100, Nanoprobes, Yaphank, NY and biotinylated donkey anti-rat, used at 1:200, Jackson Immuno Research, West Grove, PA) overnight at 4°C. The tissue was then rinsed in PBS, placed in 2% glutaraldehyde for 20 minutes, rinsed in PBS, rinsed in 2% acetate buffer, silver-intensified for four minutes (HQ silver, Nanoprobes, Yaphank, NY), then rinsed in acetate buffer and in PBS. The sections were incubated in ABC overnight at 4°C and reacted in the same manner as the single-label material. Control sections were processed in which primary antisera were omitted or in which one primary antisera was used and matched with secondary antisera raised to the other species used in our experiments. These sections showed no evidence for nonspecific DAB or immunogold labeling or for cross reactivity of our secondary's for the other primary antisera.

Double-label cocktail immunohistochemistry

In order to quantify the extent of co-localization of D_1 and D_5, tissue sections were incubated in a cocktail of the primary immunoreagents rat anti-D_1 and rabbit anti-D_5 at a dilution of 1:500 and compared to tissue sections that were incubated with rat anti-D_1 alone or rabbit anti-D_5 alone at a dilution of 1:500. This cocktail procedure has been described in detail (Muly et al., 2001), and has been used in subsequent studies (Lei et al., 2004; Mitrano and Smith, 2007; Bordelon-Glausier et al., 2008). Briefly, the tissue sections in the cocktail condition were incubated with both primary antisera, then in a cocktail of biotinylated secondary IgGs and in ABC to reveal D_1 and D_5. DAB was used as the chromagen for both D_1 and D_5. The D_1 alone and D_5 alone conditions were processed as described above.

Analysis of material

For our quantitative analyses in monkey BLA, four animals were used: three female, one male, ranging in age from 2–5 years. No differences in receptor localization related to monkey age were observed. The single-label DAB material was analyzed as previously described (Muly et al., 2003). Blocks of tissue from the BLA were made and cut in ultrathin sections that were examined using a Zeiss EM10C electron microscope. Regions of the grids containing neuropil were selected based on the presence of label and adequate ultrastructural preservation. Fields of immunoreactive elements in the neuropil were randomly selected, and images were collected at a magnification of 31,500 using a Dualvision cooled CCD camera (1300 × 1030 pixels) and Digital Micrograph software (version 3.7.4, Gatan, Inc., Pleasanton, CA). Images selected for publication were saved in TIFF format and imported into an image processing program (Canvas 8; Deneba Software, Miami, FL). The contrast was adjusted, and the images were cropped to meet size requirements. For D_1 a total of 617 micrographs representing 3,767 μm^2 of BLA were analyzed across four monkeys and a total of 1014 labeled profiles were counted. For D_5 a total of 544 micrographs representing 3,321 μm^2 of BLA were analyzed across four monkeys and a total of 994 labeled profiles were counted. For our rat studies we examined tissue from 5 adult male rats. In rat BLA, we examined 293 micrographs of tissue labeled for D_1 receptor, representing 1788 um^2 of BLA neuropil, and counted a total of 565 labeled profiles. For D_5 in the rat, we examined 244 micrographs, representing 1489 um^2 of BLA neuropil, and counted 479 labeled profiles.

On each micrograph, DAB-labeled profiles were identified and classified as spines, dendrites, terminals, axons, glia or unknown based on ultrastructural criteria (Peters et al., 1991) as previously described (Muly et al., 2003). Profiles that could not be clearly characterized based on these criteria were considered unknown profiles. The number of

immunoreactive profiles was tabulated and the distributions (excluding the unknown profiles) compared with a Chi-square analysis.

For the analysis of the immunogold/DAB, we examined ultrathin sections from the surface of each block where both immunoperoxidase label and immunogold label were visible. Because immunogold label can be noisy, we sought to avoid false-positive labeling by avoiding the very surface of each block, where non-specific gold particles tend to accumulate. We compared the immunogold label in a given structure to the surrounding background level of immunogold labeling, as well as the size of the silver intensified gold particles. If the profile qualitatively contained more immunogold label than the background level, we deemed that acceptable immunogold labeling.

For the cocktail double-label experiments in monkey, blocks of tissue from BLA were made for the D_1/D_5 cocktail condition, D_1 alone and D_5 alone conditions. Fields of the neuropil were randomly selected, and images were collected at a magnification of 20,000. An ANOVA sample size analysis (SigmaStat, Version 2.03, SPSS Inc.) indicated that the minimum sample size required to have a statistical power of 80% and a minimum detectable difference in group means of five was 474 images; therefore, we analyzed 629 images in the D_1 alone condition, 489 images in the D_5 alone condition and 572 images in the D_1/D_5 cocktail condition. In each experimental condition, the number of images analyzed from each monkey was similar. The images were coded and the analysis of these images was performed by an experimenter blind to the identity of the material until all analysis was complete. On each micrograph, spines and axon terminals were identified using the previously described ultrastructural criteria (Peters et al., 1991), then classified as immunopositive or immunonegative, and the percentage of identified spines or terminals that were immunopositive was calculated. The mean percentage of immunopositive spines and axon terminals were tabulated for each condition and compared across antigen conditions using an ANOVA. The results are reported as mean ± standard error.

***In Vitro* Brain Slice Experiments—**The methods for obtaining *in vitro* brain slices were similar to those described previously in rodents (Rainnie, 1999; Rainnie et al., 2006). Briefly, blocks of unfixed amygdala tissue were placed into oxygenated ice cold “cutting” aCSF (130 mM NaCl, 30 mM $NaHCO_3$, 3.5 mM KCl, 1.1 mM KH_2PO_4, 6 mM $MgCl_2$, 1 mM $CaCl_2$, 10 mM glucose) supplemented with 5 mM kynurenic acid to minimize glutamate-induced neurotoxicity. Tissue blocks were then glued to the stage of an OTS 4000 vibratome (Electron Microscopy Instruments) and 350 μm coronal slices of monkey amygdala were sectioned and placed in oxygenated “cutting” aCSF at 32°C for 1 hour to recover from the sectioning procedure prior to experimentation. Slices were then transferred to control aCSF of the following composition: NaCL 130 mM, 30 mM $NaHCO_3$, 3.5 mM KCl, 1.1 mM KH_2PO_4, 1.3 mM $MgCl_2$, 2.5 mM $CaCl_2$, 10 mM glucose for at least 30 minutes prior to the onset of whole-cell patch clamp recording.

Electrophysiological Recordings—Individual slices containing the BLA were placed in a Warner Series 20 recording chamber (Warner Instruments, Hamden, CT) mounted on the fixed stage of a Leica DM-LFS microscope (Leica Microsystems). Slices were fully submerged and continuously perfused at a rate of 1–2 ml per min with heated (32°C) and oxygenated control ACSF. Neurons were visualized using infrared (IR) illumination and a 40X water immersion objective (Leica Microsystems). Images were captured using an IR sensitive charge-coupled device (CCD) digital camera (Orca ER, Hamamatsu, Tokyo Japan) coupled to a Meteor-II video frame grabber (Matrox Electronic Systems Ltd, Dorval, Canada), and displayed on a computer monitor using Simple PCI 6.11 software (Compix Inc., Cranberry Township, PA).

For whole-cell patch-clamp recording, thin walled borosilicate glass patch electrodes (WPI, Sarasota, Fl.) were pulled on a Flaming/Brown micropipette puller (Model P-97, Sutter Instruments). Patch electrodes had resistances ranging from 4–8 MΩ, when filled with a standard patch solution that contained (in mM): K-Gluconate (138), KCl (2), $MgCl_2$ (3), phosphocreatine (5), K-ATP (2), NaGTP (0.2), HEPES (10). The patch recording solution was adjusted to a pH of 7.3 with KOH and had a final osmolarity of 280 mOsm. Whole-cell patch clamp recordings were obtained as previously described (Rainnie et al. 2004), using an Axopatch-1D amplifier (Molecular Devices, Sunnyvale, CA), a Digidata 1320A A–D interface, and pClamp 9.2 software (Molecular Devices). In cell-attached mode, patch electrode seal resistance was considered acceptable if it was >1.5 GΩ. Whole-cell patch-clamp configuration was established in current-clamp mode and neurons were excluded from analysis if they showed a resting membrane potential (Vm) more positive than −55 mV, and/or had an action potential that did not overshoot > +5 mV. Data from current-clamp recordings were sampled at 10 kHz and filtered at 5 kHz.

To examine the current-voltage relationship of the response to drug application, voltage ramps were applied from −100 to 0 mV at a rate of 10 mV/s, before, during, and after drug application. During drug application, voltage ramps were applied only after a steady-state drug response had been achieved. Steady-state whole-cell currents were elicited from a holding potential of −60 mV unless otherwise stated. Projection neurons were tested for their response to bath application of dopamine (DA, 50 μM), and the D1 receptor selective agonist, (1R,3S)-1-(aminomethyl)-3,4-dihydro-5,6-dihydroxy-3-phenyl-1H-2-benzopyran (A68930, 50 μM).

To examine the effects of DA on stimulus-evoked postsynaptic potentials, a concentric stimulating electrode (FHC, Bowdoinham, ME) was placed in the white matter tract immediately adjacent to the recorded neuron, and close to the fiber tract of the external capsule immediately adjacent to the BLA. Postsynaptic currents were elicited orthodromically using 5 low intensity 150 μs square-wave pulses administered once every 5 s. Unless stated otherwise, all synaptic data shown are the average of 5 consecutive stimuli.

Miniature spontaneous excitatory postsynaptic currents (mEPSCs) were recorded at a holding potential of −60 mV in the presence of tetrodotoxin (TTX, 1 μM) and 6-imino-3-(4-methoxyphenyl)-1(6*H*)-pyridazinebutanoic acid hydrobromide (SR 95531; Gabazine, 5 μM) to block fast $GABA_A$ receptor-mediated inhibitory transmission. All drugs were purchased from Sigma-Aldrich (St. Louis, MO), except for A68930 that was purchased from Tocris Cookson Inc, (Ellisville, MO). Drugs were applied by gravity perfusion at the required concentration in the circulating ACSF.

Single Cell RT-PCR—After obtaining the basic electrophysiological properties of recorded neurons, the cell cytoplasm was aspirated into the recording pipette under visual control, by applying gentle negative pressure. The capillary glass used for making the pipette was previously autoclaved and the pipette contained RNase free patch solution. After aspiration of the neuron the electrode tip was broken off and the contents were expelled into an eppendorf tube containing 1.5 μl of cell lysis buffer [1XPCR buffer II (Applied Biosystems, Foster City, CA), 1.5 mM $MgCl_2$ (Applied Biosystems), 0.5% NP40 (USB corporation, Cleveland, OH), 5 mM DTT (Invitrogen, Carlsbad, CA), 50U/μl RNase Inhibitor (Invitrogen), 10 ng/μl primer $V1(dT)_{24}$ and 2.5 mM dNTP mix (Invitrogen)] by applying positive pressure. After 15s centrifugation, the tubes was incubated in water bath at 70°C for 90s, and then immediately put on ice for 1 min. A 0.3μl volume of Reverse Transcriptase (RT) mixture [200 U/μl SuperScript III (Invitrogen), 50 U/μl RNase Inhibitor and 6 μg/μl T4 gene 32 protein (Roche, Basel, Switzerland)] was added to each reaction tube, which were then incubated at 50°C for 5 min, followed by heat-inactivation at 70°C

for 10 min. The tubes were immediately put on ice for 1 min, and after 15 s centrifugation, 1 μl of Exonuclease I mixture [1X Exonuclease I buffer and 0.5 U/μl Exonuclease I (NewEngland BioLabs, Ipswich, MA)] was added to each tube. The reaction mixture was then incubated at 37°C for 30 min, heat-inactivated at 80°C for 25 min, and then placed on ice for 1 min. Next, 6 μl of terminal deoxynucleotidyl transferase (TdT) mixture [1X PCR buffer II, 25 mM $MgCl_2$ (Qiagen Germantown, MD), 100 mM dATP (Invitrogen), 2 U/μl RNaseH (Invitrogen) and 15 U/μl TdT (Invitrogen)] was added to each tube, and the mixture was incubated at 37°C for 15 min followed by heat-inactivation at 70°C for 10 min. The RT product was stored at −20°C before further processing. The RT product in each tube (~13 μl) was divided into four 0.2 ml thin walled PCR tubes (3 μl each). Then, 19 μl of PCR mixture I [1X Buffer (Qiagen), 10 mM dNTP mix, 1 μg/μl primer V3 $(dT)_{24}$ and 0.05 U/μl Taq DNA Polymerase (Qiagen)] was added to each tube for the first round of PCR: 95 °C for 3 min, 50°C for 2 min and 72°C for 3 min. The tubes were immediately put on ice for 1 min, and 19 μl of PCR mixture II was added, with a composition similar to that of PCR buffer I except that primer V3 $(dT)_{24}$ was replaced with the primer V1 $(dT)_{24}$. The sequence of V1 $(dT)_{24}$ and V3$(dT)_{24}$ primer was 5'ATA TGG ATC CGG CGC GCC GTC GAC TTT TTT TTT TTT TTT TTT TTT TTT-3' and 5'-ATA TCT CGA GGG CGC GCC GGA TCC TTT TTT TTT TTT TTT TTT TTT TTT-3' (Kurimoto et al., 2006). A 20-cycle PCR amplification was then performed 95 °C for 30 s, 67°C for 1 min and 72°C for 3 min with a 6 s extension per cycle using PTC-200 Peltier thermal cycler (MJ Research). The amplified cDNA from each cell was screened for the expression of glyceraldehyde-3-phosphate dehydrogenase (GAPDH) as a positive control. The amplified cDNA from GAPDH positive cells was subjected to another amplification step using 2 μl of cDNA from each cell as a template and 100 nM of each of the primers. All the primers described in this paper were purchased from GenBank sequences with commercially available Oligo software (IDT Tools, Coralville, IA). The following primers were used: GAPDH, 5'-GCC ATC AAC GAC CCC TTC AT-3'and 5'-TTC ACA CCC ATC ACA AAC AT-3' (315 bp product; GenBank accession no M17701); D1R-5'-CAG TCC ATG CCA AGA ATT GCC AGA-3' and 5' –AAT CGA TGC AGA ATG GCT GGG TCT-3' (225bp product; GenBank accession no M35077); D5R-5'-AGT CGT GGA GCC TAT GAA CCT GAC-3' and 5'- GCG TCG TTG GAG AGA TTT GAG ACA-3' (517bp product; GenBank accession no M69118). The PCR master mix was comprised of 10X PCR Buffer, 3 mM $MgCl_2$, 10 mM dNTPs, 2.5 U of Taq DNA Polymerase in a final volume of 20 μl. PCR was performed using a 10 min hot start at 95°C followed by a 40 cycle program for GAPDH and D1 (94 °C for 40 s, 56°C for 40 s and 72°C for 1 min), for D5 (94 °C for 1 min, 58°C for 1 min and 72°C for 1.5 min). PCR products were visualized by staining with ethidium bromide and separated by electrophoresis in 1% agarose gel.

Results

Pattern of Localization of D1R subtypes in Primate Amygdala

D_1-immunoreactivity (-IR) is present throughout the amygdala but is heterogeneously distributed (Fig. 1A and B). D_1-IR is robust in the BLA and lateral subdivisions of the amygdala, is found at moderate levels in the basomedial subdivision and is relatively weak in the central nucleus. Of particular note, there are densely stained patches of D_1-IR found between the subdivisions of the amygdala, especially between the central nucleus and the more ventral regions. These appear to be analogous to the intercalated cell groups identified in rat amygdala and which stain intensely for D_1 (Fuxe et al., 2003). D_5-IR is also present throughout the amygdala but appears more homogeneous than D_1, though the central nucleus is more lightly labeled than the rest of the structure (Fig. 1C and D). When examined at higher magnification, D_1-IR in the BLA is most intense in a perinuclear reticular network in cell bodies (Fig. 2A), which has previously been associated with

labeling in the Golgi apparatus (Muly et al., 1998; Bordelon-Glausier et al., 2008). In addition, D_1-IR can also be identified within the soma outside of this reticular network as well as in the neuropil where a light, granular or punctate pattern can be identified. Within the dense patches of D_1-IR interposed between the central nucleus and ventral amygdala, neuropil staining is more intense and immunoreactive fibers can be identified (Fig. 2B). D_5-IR in the BLA is found in cell bodies and in the neuropil with both puncta and processes labeled (Fig. 2C).

Subcellular Distribution of D1R in Primate BLA

We next examined the localization of D1Rs in the primate BLA in material prepared for electron microscopy. As anticipated from the light microscopy examination, both D_1- and D_5-IR are found in neuronal cell bodies in the BLA. As previously reported in the prefrontal cortex, somatic D_1-IR is concentrated in the Golgi apparatus of neurons (Fig. 3A); however, unlike cortical neurons, D_1-IR is also found associated with other internal membranes in BLA neurons (Fig. 3B). In contrast with D_1-, D_5-IR is not localized to Golgi complexes, but rather is found associated with other internal membranes (Fig. 3C). D_5-IR can also be observed in proximity to the plasma membrane, occasionally adjacent to subsurface membrane structures (Fig. 3C), analogous to previous reports in the prefrontal cortex (Paspalas and Goldman-Rakic, 2004).

The bulk of immunoreactivity for both D1R subtypes is found in the neuropil and both were widely distributed. Both D_1- and D_5-IR were commonly seen in dendritic structures, including spines (Fig. 4A and B) and dendritic shafts (Fig. 4C–E). These immunoreactive shafts included dendrites that received asymmetric (Fig. 4D) and symmetric synapses (Fig. 4E). Glial processes were also observed with label for both D_1 and D_5 (Fig. 4F). In addition, both D_1- and D_5-IR were seen in preterminal axons and axon terminals (Fig. 5). Both D1Rs were found in a diverse group of terminals, including those making asymmetric (Fig. 5A and B) and symmetric synapses (Fig. 5C) as well as those containing prominent dense core vesicles (Fig. 5B). In addition, D_1-IR terminals were occasionally observed making asymmetric synapses onto D_1-IR dendritic spines (Fig. 5D and E). In order to determine if the patterns of neuropil distribution differed for the two D1R receptors, we quantified their distribution in the BLA. We examined randomly collected images of neuropil labeling for each receptor and identified 918 D_1-IR profiles and 903 D_5-IR profiles. The patterns of D_1 and D_5 labeling confirmed our impression of widespread distributions and differed significantly (Fig. 6; $\chi^2 = 79.679$; $p<0.0001$). Post-hoc testing revealed that D_1 immunoreactivity was more commonly found in dendritic shafts, while D_5 immunoreactivity was more commonly found in axon terminals and preterminal axons.

Our previous work in rhesus monkey prefrontal cortex has indicated an extensive overlap of D_1 and D_5 receptors in populations of dendritic spines and axon terminals (Bordelon-Glausier et al., 2008). Because both receptors are found commonly in these structures in the BLA as well, we used double-label pre-embedding immunogold and immunoperoxidase methods to determine if the two receptors colocalized in the BLA. While the signal obtained with the pre-embedding immunogold method is weaker than that seen with immunoperoxidase, we did achieve specific labeling, as evidenced by D_1 gold labeling in Golgi complexes (Fig. 7A). Double labeled dendrites were frequently observed, regardless of which receptor was labeled with gold (Fig. 7B and C). Gold signal in spines and terminals was weaker and sometimes difficult to distinguish from background staining; however, examples of D_1/D_5 double labeled spines and terminals were observed (Fig. 7D–G).

In order to quantify the degree to which the two receptors co-localize in spines and axon terminals, we used a cocktail labeling approach which we have previously used to identify overlapping distributions of proteins (Muly et al., 2001; Bordelon-Glausier et al., 2008). The

advantage of this method is that the labeling method used for each receptor has the same sensitivity and penetration into tissue, thus minimizing the effect of false negative labeling which is problematic for pre-embedding immunogold labeling. We randomly imaged material labeled with antiserum to D_1, D_5 or a cocktail of antisera to both receptors and calculated the percentage of spines and terminals labeled for each receptor individually as well as for the two receptors combined. We found that 24.1% +/−1.3% of spines in the BLA contained D_1-IR, while 18.0% +/− 1.4% contained D_5-IR. The percentage of spines in the BLA labeled individually for the two receptors or the cocktail of both antisera differed significantly (Fig. 8A; $F_{2,1687} = 5.729$, $p = .0033$), and post-hoc Scheffe tests confirmed that the percentage of spines labeled for D_5 was significantly less than for D_1 ($p = .0069$) and the cocktail ($p = .0226$). However, there was no significant difference between the percentage of spines labeled for D_1 or the cocktail of D_1 and D_5 ($p = .9377$). The finding that the percentage of spines labeled by D_1 and a cocktail of D_1 and D_5 is not significantly different demonstrates that the D_5 receptor is found in a subpopulation of the D_1 positive spines. If D_1 and D_5 labeled separate populations of spines, the cocktail condition would label a higher percentage of spines than D_1 alone. This data indicates that both D_1 and D_5 are found together in approximately 18% of dendritic spines, and that D_1 is found in an additional 6% of BLA spines.

The extensive overlap of D_1 and D_5 in dendritic spines suggests that individual BLA projection neurons must co-express these receptors. We tested this hypothesis using single-cell RT-PCR on samples obtained from primate BLA projection neurons recorded in *in vitro* slices (Fig. 9). Here, we looked for the presence of D_1 and D_5 mRNA in a representative sample of 19 primate projection neurons using available primers based on the rat sequence for each gene. We were able to identify the mRNA for a housekeeping gene, glyceraldehydes-3-phosphate dehydrogenase (GAPDH), in 15/19 neurons and only these neurons were then tested for their expression of D_1 and D_5 mRNA. An mRNA signal for either D_1 or D_5 was detected in 13/15 GAPDH positive samples. An mRNA signal was detected in nine neurons each for D_1 and D_5. Significantly, 5/9 neurons had mRNA transcripts for both D_1 and D_5 receptors. These results strongly support our hypothesis that individual BLA projection neurons express both D_1 and D_5 receptors. Moreover, given the variable sensitivity of RT-PCR and our use of primers from rat, the degree of co-expression observed with this method is likely an underestimate of D_1 and D_5 co-expression.

We also performed a double-label cocktail analysis for axon terminals in the BLA, as we had for dendritic spines. We found that 3.6% +/− 0.3% of terminals in the BLA contained D_1-IR, while 6.4% +/− 0.4% contained D_5-IR. As seen for dendritic spine labeling, the percentage of axon terminals labeled for D_1, D_5 or the cocktail differed significantly (Fig. 8B; $F_{2,2021} = 15.683$, $p<.0001$), and post-hoc Scheffe tests confirmed that the percentage D_1 labeled terminals was significantly less than D_5 ($p < .0001$) and the cocktail ($p < .0001$); however, there was no significant difference between D_5 and the cocktail ($p = .8220$). Thus, as in spines there is extensive overlap between the populations of terminals that contain the two receptors. Unlike spines, in terminals, D_5 is found more frequently and our results indicate that both D_1 and D_5 are found together in approximately 3.5% of axon terminals, and that D_5 is found in an additional 3% of BLA terminals

We next examined the synaptic type and postsynaptic structures of D1R-labeled axon terminals. Of the 26 D_1 positive axon terminals which made identifiable synapses, 22 were asymmetric and four were symmetric. Sixteen of the asymmetric synapses were onto spines, while the remaining six were onto unlabeled dendrites. Three of the symmetric synapses were onto dendrites and the remaining D_1 positive axon terminal formed a symmetric synapse onto an unlabeled spine. Of the 29 D_5 positive axon terminals which made identifiable synapses, 22 were asymmetric and seven were symmetric. Twenty of the

asymmetric synapses were onto spines, while the remaining two were onto dendrites. The symmetric synapses were all onto dendrites. In addition, dense core vesicles were frequently observed both in D_1-IR (29.9%) and D_5-IR (27.3%) terminals. These data suggest that D1R are positioned to presynaptically modulate a wide variety of inputs, in particular excitatory axospinous inputs.

Actions of Dopamine and D1R in Primate BLA

To determine how D1 family receptor activation might modulate neuronal activity in the primate basolateral amygdala (BLA) we used *in vitro* whole cell patch-clamp recording from BLA projection neurons to examine the response to exogenous application of either dopamine or the D1R–selective agonist, A68930. To date no study has reported on the basic membrane properties of neurons in the primate BLA. In order to make a direct comparison between the dopamine-evoked response in rodent and primate projection neurons we first characterized some of the basic membrane properties of projection neurons in the primate BLA, a more detailed analysis of the membrane properties of these neurons is in preparation. As illustrated in Figure 10, the voltage response (upper trace) of primate BLA projection neurons to graded injection of either hyperpolarizing or depolarizing current (lower trace) is qualitatively no different from that previously reported for rodent BLA projection neurons (Rainnie et al., 1993; Sah et al., 2003; McDonald et al., 2005). In response to depolarizing current injection, primate projection neurons often fired an initial doublet of action potentials and then settled down to a relatively rhythmic firing pattern. In the hyperpolarizing direction, voltage deflections of increasing amplitude were characterized by the presence of a time-dependent depolarizing sag that increased in amplitude as the membrane potential became more negative. This depolarizing sag is characteristic of the voltage response seen in rodent BLA projection neurons following activation of the hyperpolarization-activated non-selective cation current, I_h.

Note the occurrence of spontaneous IPSPs in the voltage traces above −60 mV (Fig. 10), which reverse polarity at more negative membrane potentials. Similar to the high amplitude and long duration spontaneous IPSPs observed in rodent projections neurons that are mediated by $GABA_A$ receptor activation (Rainnie, 1999), the spontaneous IPSPs in primate projection neurons occur at a frequency of ~ 1 Hz and were blocked by prior application of the selective $GABA_A$ receptor antagonist, bicuculline methiodide (30 μM, data not shown).

An examination of the resting membrane properties and spike characteristics of revealed significant differences in some, but not all, of the properties of primate BLA projection neurons compared to those of a representative sample of rodent projection neurons (Table 1). Primate projection neurons had a significantly lower membrane input resistance (Rm; Primate = 39±5 MΩ: Rat = 71±3 MΩ; $p < 0.01$), which is consistent with them having a greater somatic surface area and a more extensive dendritic arbor. No significant difference was observed in the threshold for action potential generation, and either the rise-time or amplitude of single action potentials. However, the primate action potential half-width was significantly longer than that of the rodent (Primate = 1.1 ± 0.1 ms; Rat = 0.89 ± 0.1 ms; $p < 0.01$), which is consistent with the significantly slower decay time seen in primate projection neurons (Primate = 1.5 ± 0.1 ms: Rat = 0.92 ± 0.1 ms; $p < 0.01$). Taken together, these data suggested that primate projection neurons expressed many of the same intrinsic membrane currents that are found in projection neurons from the rat BLA, with some differences observed that are likely attributable to the larger size of primate neurons.

Given the similarities in membrane response properties between primate and rat BLA neurons, we predicted that exogenous dopamine would affect the excitability of primate BLA projection neurons in much the same way as it affects rat projection neurons. Consistent with our prediction, application of dopamine (50 μM) caused a reversible 3.8±0.2

mV depolarization of the resting membrane potential of primate projection neurons that was associated with a significant reduction (21%) in the membrane input resistance (Fig. 11 A; Control: 35±7 MΩ; Dopamine 27±7 MΩ, n = 10, $p < 0.05$). In voltage clamp mode (Fig. 11B), exogenous dopamine application was seen to elicit an inward current (59 ± 5.6 pA, n=17) that persisted in the presence of tetrodotoxin (TTX, 1 μM), and which had an apparent reversal potential of −39 ± 2.1 mV (n=17). These data are consistent with previous studies in the rat BLA in which a similar dopamine-evoked inward current observed in projection neurons was mimicked by the D1R selective agonist, dihydrexidine, and blocked by the D1R selective antagonist SCH 23390 (Levita et al., 2003; Pickel et al., 2006).

Moreover, in control aCSF application of dopamine (50 μM) routinely caused a doubling in the frequency of the spontaneous IPSPs in primate projections neurons (Fig. 12). Hence, in aCSF spontaneous $GABA_A$ receptor-mediated IPSPs occurred at a frequency of 0.85±0.2 Hz (Fig. 12A, n = 8). In the presence of dopamine (50 μM) the frequency of spontaneous IPSPs increased to 1.65± 0.3 Hz (Fig. 12 B, n = 8, $p<0.01$), and returned back to control values (0.7 ± 0. 4 Hz) following washout with aCSF (Fig 12C, n = 8). A similar increase in spontaneous IPSP frequency has been reported in projection neurons of the rat BLA (Levita et al., 2003;Kroner et al., 2005) and has been shown to result from a direct D1R–mediated excitation of local circuit interneurons.

Our localization studies found both D_1 and D_5 receptors present in axon terminals making asymmetric contacts with the spines of primate BLA projection neurons, similar to observations of the D_1 receptor in the rat BLA (Pickel et al., 2006). Consequently, we next examined the effects of exogenous application of the D1R selective agonist, A68930 (50 μM), on the amplitude and frequency of miniature excitatory postsynaptic currents (mEPSCs) recorded in primate projection neurons in the presence of TTX and GABA receptor antagonists. As illustrated in Figure 13, application of A68930 increased the frequency (control 4.8±1.1 Hz; A68930 6.8±1.7 Hz; n=6, $p<0.05$), but not the amplitude (control 14.6±0.6 pA; A68930 14.3±0.9 pA; n=6, $p>0.05$), of mEPSCs in primate projection neurons, suggesting a presynaptic site of D1R action. Prior application of the non-selective D1R antagonist (SCH23390, 20 μM), which has no effect on either the amplitude or the frequency of mEPSCs by itself, fully blocked the A69830 induced increase in mEPSC frequency (SCH 23390 3.7±0.7 Hz; A68930 in SCH23390 3.3±0.6 Hz, n=6, $p>0.05$; Fig. 14).

Subcellular Distribution of D1R in Rat BLA

Because of the similarities between what we observed of the actions of dopamine and D1R stimulation in primate BLA and what has previously been reported in rat BLA, we wanted to determine how the distribution of D1R in rat BLA compared to primate. We performed immunohistochemistry for both D_1 and D_5 in rat brain sections and quantified the distribution of these receptors in BLA. We examined randomly collected images of neuropil labeling for each receptor and identified 526 D_1-IR profiles and 451 D_5-IR profiles. Both D_1 and D_5 were widely distributed within rat BLA (Fig. 15), as we found in primate BLA. The distributions of the two receptors differed in rat BLA (χ^2= 72.371; $p<.0001$). Post-hoc testing revealed that D_1 immunoreactivity was more commonly found in dendritic spines, while D_5 immunoreactivity was more commonly found in axon terminals and glia. When we contrast the distribution of each receptor between the two species, in the rat D_1 is found more frequently in spines and preterminal axons and less commonly in dendritic shafts than we observed in primate while D_5 is found more frequently in dendrites and glia in rat and less frequently in spines compared to primate. On the other hand, the distribution of D1R in the BLA of the two species shares some significant similarities, including relatively more presynaptic localization of the D_5 receptor and relatively more postsynaptic localization of the D1 receptor.

Discussion

Dopamine activation of D1 family dopamine receptors plays a critical role in amygdala functioning. Dopamine levels are increased in the amygdala by conditioned fear stress (Yokoyama et al., 2005) and D1R activation in the BLA is necessary for the development of conditioned fear (Lamont and Kokkinidis, 1998; Nader and LeDoux, 1999; Guarraci et al., 1999; Greba and Kokkinidis, 2000; Macedo et al., 2007). The data presented here provide the first detailed description of the distribution of D1 family dopamine receptors in the primate BLA. In addition, we present physiological evidence for dopamine actions in the primate BLA that are similar to those reported in the rat. Finally, we contrast the distribution of D_1 and D_5 in the rat and monkey.

Our results demonstrate a complex and widespread distribution of both D_1 and D_5 receptors in primate BLA with both receptors found both postsynaptically in the dendritic arbor of BLA neurons and presynaptically in axon terminals and preterminal axons. Our electrophysiological data confirmed that dopamine and D1R stimulation can directly depolarize and excite both BLA projection neurons and interneurons, as well as act presynaptically in increase neurotransmitter release from glutamatergic terminals. Furthermore, while previous studies have highlighted D_1 localization in intercalated cell masses, our finding that one quarter of dendritic spines in the BLA contain either D_1 or D_1 and D_5 show that dopamine acting on these receptors will have powerful effects by directly modulating the excitability of BLA projection neurons. Thus, dopamine's actions in primate amygdala are a complex mix of post- and presynaptic actions at several sites in intra-amygdala circuits.

The finding that the D_5 receptor is found in significant numbers of BLA spines, though the D_1 receptor is more abundant is significant given the observation that D1R agonists do not appear to couple to adenylate cyclase the amygdala (Leonard et al., 2003), but rather couple to phosphoinositol hydrolysis (Undie and Friedman, 1990). Studies from transgenic mice have suggested that D1R coupling to phospholipase C is mediated by the D_5, but not the D_1 receptor (Friedman et al., 1997; Sahu et al., 2008). Our study shows significant D_1 receptor localization in both monkey and rat BLA, thus the alternate coupling observed in the amygdala is not solely due to a different D1R subtype present there. It remains to be determined if the different D1R signaling in the amygdala is due to different availability of signal transduction proteins there or possible heterodimerization of D1R subtypes with each other or another receptor.

Our comparison of the distributions of the D_1 and D_5 receptors in monkey BLA shows patterns that are in general similar but with some significant differences. D_1 is found more frequently in dendrites than D_5, while D_5 is more frequently found in presynaptic compartments. The two D1R subtypes are co-expressed in BLA projection neurons and overlap extensively in spines and terminals but with D_1 predominant in spines while D_5 is predominant in terminals. The significance of this finding depends on the functional differences between the two D1R subtypes. Efforts to determine these differences have been hampered by a lack of pharmacological tools that adequately differentiate the two receptors. Despite this, a growing body of evidence points to important differences between the two. Investigators using transgenic mice or antisense oligonucleotide injections have found that D_5, but not D_1 receptors, are necessary for cocaine discrimination as well as dopamine-evoked acetylcholine release in the hippocampus (Filip et al., 2000; Hersi et al., 2000; Laplante et al., 2004). Furthermore, D_1 directly interacts with the NMDA receptor (Lee et al., 2002), while D_5 directly interacts with the $GABA_A$ receptor (Liu et al., 2000). Intriguingly, the two D1R subtypes appear to play differential roles in modulating synaptic plasticity. Corticostriatal long-term potentiation is disrupted in D_1 knockout mice, while

blockade of the remaining D_5 receptors prevents induction of long-term depression (Centonze et al., 2003). In particular, the D_5 receptor has a 10 fold higher affinity for dopamine, the endogenous ligand (Sunahara et al., 1991; Weinshank et al., 1991). This observation, coupled with the D_5 receptor's relatively preferential localization in presynaptic compartments suggests that in the BLA presynaptic D1R effects might dominate at low levels of dopamine release and that as the activity of dopaminergic inputs increased, postsynaptic actions might become more prominent.

This study also allowed us to compare the distributions of D1R subtypes between two species, the rhesus monkey and rat. Previously, only the localization of the D_1 subtype in rat amygdala has been examined qualitatively and with somewhat divergent results. Pickel and colleagues (2006) reported D_1-IR mainly in cell bodies and dendrites, with spines and axon terminals seen more rarely. Alternately, Pinto and Sesack (2008) reported D_1-IR was most commonly seen in dendritic spines, with dendritic shafts, axonal elements and glia less commonly seen. Our data confirmed that label is more common in the dendritic arbor than the axon arbor with both spines and dendrites being commonly labeled, with presynaptic and glial localization relatively less common. In comparing the localization profiles we observed in monkey and rat, there were significant similarities noted. Both receptors were widely distributed in both species. Labeling was more common in the dendritic arbor for D_1 in both species and in the axonal arbor for D_5 in both species. As discussed above, D_5 has a higher affinity for dopamine than D_1 and our results in rat and monkey suggest that presynaptic action at a low concentration of dopamine is an important and conserved aspect of dopaminergic regulation of the BLA. There were some differences between the two species, in particular D_1 was found more frequently in spines and less so in dendrites in rats, while D_5 was found less frequently in spines and more so in dendrites in rats compared to monkeys. Our physiological data in monkey was notable for its similarities with previous studies in rat. In future studies it will be interesting to examine whether there are any major differences in the postsynaptic responses to dopamine between the two species.

Acknowledgments

This work was supported by a Merit Award from the Office of Research and Development, Department of Veterans Affairs to ECM; MH069852 from the National Institutes of Health to DGR and BFU 2006-00306 from the Ministerio de Educacion y Ciencia to ZUK; and the Center for Behavioral Neuroscience (NSF agreement IBN-9876754), and by an NIH/NCRR base grant (P51RR000165) to Yerkes National Primate Research Center.

Reference List

Berglind WJ, Case JM, Parker MP, Fuchs RA, See RE. Dopamine D1 or D2 receptor antagonism within the basolateral amygdala differentially alters the acquisition of cocaine-cue associations necessary for cue-induced reinstatement of cocaine-seeking. Neurosci 2006;137:699–706.

Bordelon-Glausier JR, Khan ZU, Muly EC. Quantification of D1 and D5 dopamine receptor localization in layers I, III, and V of Macaca mulatta prefrontal cortical area 9: coexpression in dendritic spines and axon terminals. J Comp Neurol 2008;508:893–905. [PubMed: 18399540]

Centonze D, Grande C, Saulle E, Martin AB, Gubellini P, Pavon N, Pisani A, Bernardi G, Moratalla R, Calabresi P. Distinct roles of D1 and D5 dopamine receptors in motor activity and striatal synaptic plasticity. J Neurosci 2003;23:8506–8512. [PubMed: 13679419]

Ciccocioppo R, Sanna PP, Weiss F. Cocaine-predictive stimulus induces drug-seeking behavior and neural activation in limbic brain regions after multiple months of abstinence: Reversal by D1 antagonists. Proceedings of the National Academy of Sciences 2001;98:1976–1981.

Civelli O, Bunzow JB, Grandy DK. Molecular diversity of the dopamine receptors. Annual Rev Pharmacol Toxicol 1993;32:281–307. [PubMed: 8494342]

de la Mora MP, Cardenas-Cachon L, Vazquez-Garcia M, Crespo-Ramirez M, Jacobsen K, Hoistad M, Agnati L, Fuxe K. Anxiolytic effects of intra-amygdaloid injection of the D1 antagonist SCH23390 in the rat. Neurosci Lett 2005;377:101–105. [PubMed: 15740845]

Filip M, Thomas ML, Cunningham KA. Dopamine D5 receptors in nucleus accumbens contribute to the detection of cocaine in rats. J Neurosci 2000;20:RC98. [PubMed: 11000198]

Friedman E, Jin LQ, Cai GP, Hollon TR, Drago J, Sibley DR, Wang HY. D_1-like dopaminergic activation of phosphoinositide hydrolysis is independent of D_{1A} dopamine receptors: Evidence from D_{1A} knockout mice. Molecular Pharmacology 1997;51:6–11. [PubMed: 9016340]

Fuxe K, Jacobsen KX, Hoistad M, Tinner B, Jansson A, Staines WA, Agnati LF. The dopamine D1 receptor-rich main and paracapsular intercalated nerve cell groups of the rat amygdala: relationship to the dopamine innervation. Neurosci 2003;119:733–746.

Gingrich JA, Caron MG. Recent advances in the molecular biology of dopamine receptors. Annu Rev Neurosci 1993;16:299–321. [PubMed: 8460895]

Greba Q, Kokkinidis L. Peripheral and intraamygdalar administration of the dopamine D1 receptor antagonist SCH 23390 blocks fear-potentiated startle but not shock reactivity or the shock sensitization of acoustic startle. Behav Neurosci 2000;114:262–272. [PubMed: 10832788]

Guarraci FA, Frohardt RJ, Kapp BS. Amygdaloid D1 dopamine receptor involvement in Pavlovian fear conditioning. Brain Res 1999;827:28–40. [PubMed: 10320690]

Hersch SM, Ciliax BJ, Gutekunst C-A, Rees HD, Heilman CJ, Yung KKL, Bolam JP, Ince E, Yi H, Levey AI. Electron microscopic analysis of D1 and D2 dopamine receptor proteins in the dorsal striatum and their synaptic relationships with motor corticostriatal afferents. J Neurosci 1995;15:5222–5237. [PubMed: 7623147]

Hersi AI, Kitaichi K, Srivastava LK, Gaudreau P, Quirion R. Dopamine D-5 receptor modulates hippocampal acetylcholine release. Brain Res Mol Brain Res 2000;76:336–340. [PubMed: 10762709]

Jacobsen KX, Hoistad M, Staines WA, Fuxe K. The distribution of dopamine D1 receptor and mu-opioid receptor 1 receptor immunoreactivities in the amygdala and interstitial nucleus of the posterior limb of the anterior commissure: relationships to tyrosine hydroxylase and opioid peptide terminal systems. Neurosci 2006;141:2007–2018.

Khan ZU, Gutierrez A, Martin R, Penafiel A, Rivera A, de la CA. Dopamine D5 receptors of rat and human brain. Neurosci 2000;100:689–699.

Kroner S, Rosenkranz JA, Grace AA, Barrionuevo G. Dopamine modulates excitability of basolateral amygdala neurons in vitro. J Neurophysiol 2005;93:1598–1610. [PubMed: 15537813]

Kurimoto K, Yabuta Y, Ohinata Y, Ono Y, Uno KD, Yamada RG, Ueda HR, Saitou M. An improved single-cell cDNA amplification method for efficient high-density oligonucleotide microarray analysis. Nucleic Acids Res 2006;34:e42. [PubMed: 16547197]

Lamont EW, Kokkinidis L. Infusion of the dopamine D1 receptor antagonist SCH 23390 into the amygdala blocks fear expression in a potentiated startle paradigm. Brain Res 1998;795:128–136. [PubMed: 9622611]

Laplante F, Sibley DR, Quirion R. Reduction in acetylcholine release in the hippocampus of dopamine D5 receptor-deficient mice. Neuropsychopharmacol 2004;29:1620–1627.

Lee FJ, Xue S, Pei L, Vukusic B, Chery N, Wang Y, Wang YT, Niznik HB, Yu XM, Liu F. Dual regulation of NMDA receptor functions by direct protein-protein interactions with the dopamine D1 receptor. Cell 2002;111:219–230. [PubMed: 12408866]

Lei W, Jiao Y, Del Mar N, Reiner A. Evidence for differential cortical input to direct pathway versus indirect pathway striatal projection neurons in rats. J Neurosci 2004;24:8289–8299. [PubMed: 15385612]

Leonard SK, Anderson CM, Lachowicz JE, Schulz DW, Kilts CD, Mailman RB. Amygdaloid D1 receptors are not linked to stimulation of adenylate cyclase. Syn 2003;50:320–333.

Levita L, Mania I, Rainnie DG. Dopamine activates multiple conductances in the basolateral amygdala. Society for Neuroscience Abstract Viewer and Itinerary Planner Program#336 2003:19.

Liu F, Wan Q, Pristupa ZB, Yu XM, Wang YT, Niznik HB. Direct protein-protein coupling enables cross-talk between dopamine D5 and gamma-aminobutyric acid A receptors. Nat 2000;403:274–280.

Loretan K, Bissiere S, Luthi A. Dopaminergic modulation of spontaneous inhibitory network activity in the lateral amygdala. Neuropharmacology 2004;47:631–639. [PubMed: 15458834]

Macedo CE, Martinez RC, Albrechet-Souza L, Molina VA, Brandao ML. 5-HT2- and D1-mechanisms of the basolateral nucleus of the amygdala enhance conditioned fear and impair unconditioned fear. Behav Brain Res 2007;177:100–108. [PubMed: 17126419]

Maltais S, te C, Drolet G, Falardeau P. Cellular colocalization of dopamine D1 mRNA and D2 receptor in rat brain using a D2 dopamine receptor specific polyclonal antibody. Prog Neuropsychopharmacol Biol Psychiatry 2000;24:1127–1149. [PubMed: 11131177]

Mansour A, Meador-Woodruff JH, Zhou QY, Civelli O, Akil H, Watson SJ. A comparison of D1 receptor binding and mRNA in rat brain using receptor autoradiographic and in situ hybridization techniques. Neurosci 1991;45:359–371.

Marowsky A, Yanagawa Y, Obata K, Vogt KE. A specialized subclass of interneurons mediates dopaminergic facilitation of amygdala function. Neuron 2005;48:1025–1037. [PubMed: 16364905]

McDonald AJ, Mascagni F, Mania I, Rainnie DG. Evidence for a perisomatic innervation of parvalbumin-containing interneurons by individual pyramidal cells in the basolateral amygdala. Brain Res 2005;1035:32–40. [PubMed: 15713274]

Mitrano DA, Smith Y. Comparative analysis of the subcellular and subsynaptic localization of mGluR1a and mGluR5 metabotropic glutamate receptors in the shell and core of the nucleus accumbens in rat and monkey. J Comp Neurol 2007;500:788–806. [PubMed: 17154259]

Montague DM, Striplin CD, Overcash JS, Drago J, Lawler CP, Mailman RB. Quantification of D1B(D5) receptors in dopamine D1A receptor-deficient mice. Syn 2001;39:319–322.

Muly EC, Greengard P, Goldman-Rakic PS. Distribution of protein phosphatases-1α and −1γ1 and the D1 dopamine receptor in primate prefrontal cortex: Evidence for discrete populations of spines. J Comp Neurol 2001;440:261–270. [PubMed: 11745622]

Muly EC, Maddox M, Smith Y. Distribution of mGluR1α and mGluR5 immunolabeling in primate prefrontal cortex. J Comp Neurol 2003;467:521–535. [PubMed: 14624486]

Muly EC, Szigeti K, Goldman-Rakic PS. D_1 receptor in interneurons of macaque prefrontal cortex: distribution and subcellular localization. J Neurosci 1998;18:10553–10565. [PubMed: 9852592]

Nader K, LeDoux JE. Inhibition of the mesoamygdala dopaminergic pathway impairs the retrieval of conditioned fear associations. Behav Neurosci 1999;113:891–901. [PubMed: 10571473]

Paspalas CD, Goldman-Rakic PS. Microdomains for dopamine volume neurotransmission in primate prefrontal cortex. J Neurosci 2004;24:5292–5300. [PubMed: 15190100]

Peters, A.; Palay, SL.; Webster, Hd. The Fine Structure of the Nervous System: Neurons and Their Supporting Cells. New York: Oxford University Press; 1991.

Pickel VM, Colago EE, Mania I, Molosh AI, Rainnie DG. Dopamine D1 receptors co-distribute with N-methyl-D-aspartic acid type-1 subunits and modulate synaptically-evoked N-methyl-D-aspartic acid currents in rat basolateral amygdala. Neurosci 2006;142:671–690.

Pinto A, Sesack SR. Ultrastructural analysis of prefrontal cortical inputs to the rat amygdala: spatial relationships to presumed dopamine axons and D1 and D2 receptors. Brain Struct Funct. 2008

Rainnie DG. Serotonergic modulation of neurotransmission in the rat basolateral amygdala. J Neurophysiol 1999;82:69–85. [PubMed: 10400936]

Rainnie DG, Asprodini EK, Shinnick-Gallagher P. Intracellular recordings from morphologically identified neurons of the basolateral amygdala. J Neurophysiol 1993;69:1350–1362. [PubMed: 8492168]

Rainnie DG, Mania I, Mascagni F, McDonald AJ. Physiological and morphological characterization of parvalbumin-containing interneurons of the rat basolateral amygdala. J Comp Neurol 2006;498:142–161. [PubMed: 16856165]

Rosenkranz JA, Grace AA. Cellular mechanisms of infralimbic and prelimbic prefrontal cortical inhibition and dopaminergic modulation of basolateral amygdala neurons in vivo. J Neurosci 2002;22:324–337. [PubMed: 11756516]

Sah P, Faber ES, Lopez dA, Power J. The amygdaloid complex: anatomy and physiology. Physiol Rev 2003;83:803–834. [PubMed: 12843409]

Sahu A, Tyeryar KR, Vongtau HO, Sibley DR, Undieh AS. D5 Dopamine Receptors are Required for Dopaminergic Activation of Phospholipase C. Mol Pharmacol. 2008

Scibilia RJ, Lachowicz JE, Kilts CD. Topographic nonoverlapping distribution of D1 and D2 dopamine receptors in the amygdaloid nuclear complex of the rat brain. Syn 1992;11:146–154.

See RE, Fuchs RA, Ledford CC, McLaughlin J. Drug addiction, relapse, and the amygdala. Ann N Y Acad Sci 2003;985:294–307. [PubMed: 12724166]

See RE, Kruzich PJ, Grimm JW. Dopamine, but not glutamate, receptor blockade in the basolateral amygdala attenuates conditioned reward in a rat model of relapse to cocaine-seeking behavior. Psychopharmacology (Berl) 2001;154:301–310. [PubMed: 11351937]

Smiley JF, Levey AI, Ciliax BJ, Goldman-Rakic PS. D_1 dopamine receptor immunoreactivity in human and monkey cerebral cortex: predominant and extrasynaptic localization in dendritic spines. Proc Natl Acad Sci USA 1994;91:5720–5724. [PubMed: 7911245]

Sunahara RK, Guan H-C, O'Dowd BF, Seeman P, Laurier LG, Ng G, George SR, Torchia J, Van Tol HHM, Niznik HB. Cloning of the gene for a human dopamine D_5 receptor with a higher affinity for dopamine than D_1. Nat 1991;350:614–619.

Tiberi M, Jarvie KR, Silvia C, Falardeau P, Gingrich JA, Godinot N, Bertrand L, Yang-Feng TL, Fremeau RT Jr, Caron MG. Cloning, molecular characterization, and chromosomal assignment of a gene encoding a second D1 dopamine receptor subtype: differential expression pattern in rat brain compared with the D1A receptor. Proc Natl Acad Sci U S A 1991;88:7491–7495. [PubMed: 1831904]

Undie AS, Friedman E. Stimulation of a dopamine D1 receptor enhances inositol phosphates formation in rat brain. J Pharmacol Exp Ther 1990;253:987–992. [PubMed: 1972756]

Weinshank RL, Adham N, Macchi M, Olsen MA, Branchek TA, Hartig PR. Molecular cloning and characterization of a high affinity dopamine receptor (D1 beta) and its pseudogene. J Biol Chem 1991;266:22427–22435. [PubMed: 1834671]

Yamamoto R, Ueta Y, Kato N. Dopamine induces a slow afterdepolarization in lateral amygdala neurons. J Neurophysiol 2007;98:984–992. [PubMed: 17553953]

Yokoyama M, Suzuki E, Sato T, Maruta S, Watanabe S, Miyaoka H. Amygdalic levels of dopamine and serotonin rise upon exposure to conditioned fear stress without elevation of glutamate. Neurosci Lett 2005;379:37–41. [PubMed: 15814195]

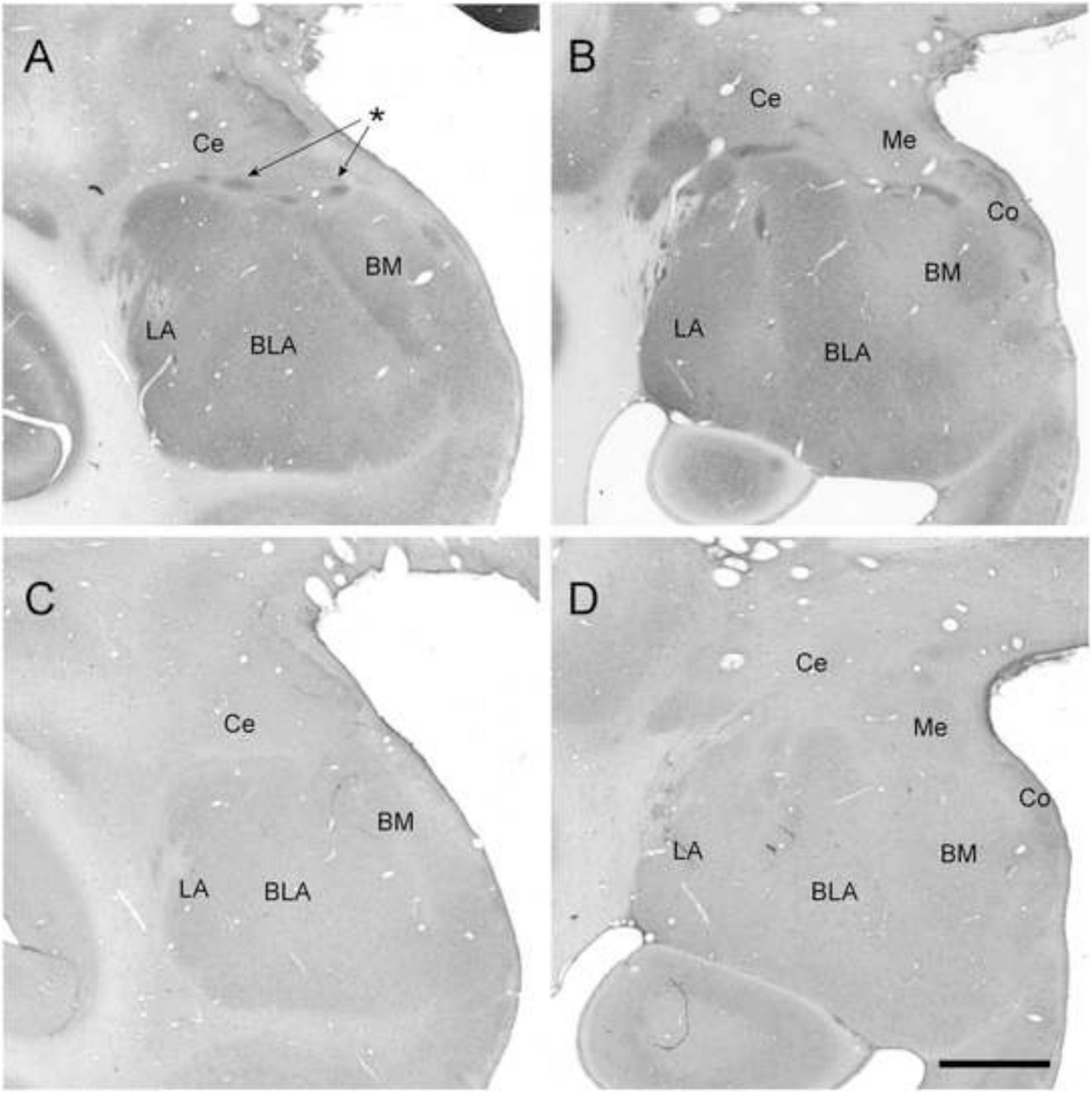

Figure 1.

The pattern of D1 family receptor labeling in the monkey amygdala. **A, B**: The pattern of D_1-IR in rostral and caudal sections of the amygdala respectively. Note the presence of small, densely labeled patches found between Ce and the other subdivisions of the amygdala (examples indicated by asterisks). **C, D**: The pattern of D_5-IR in rostral and caudal sections of the amygdala respectively. Abreviations used: BLA- basolateral amygdala complex, BM- Basomedial nucleus, Ce- Central nucleu, Co- Cortical nucleus, La- lateral nucleus, Me- Medial nucleus. Scale bar is 2 mm.

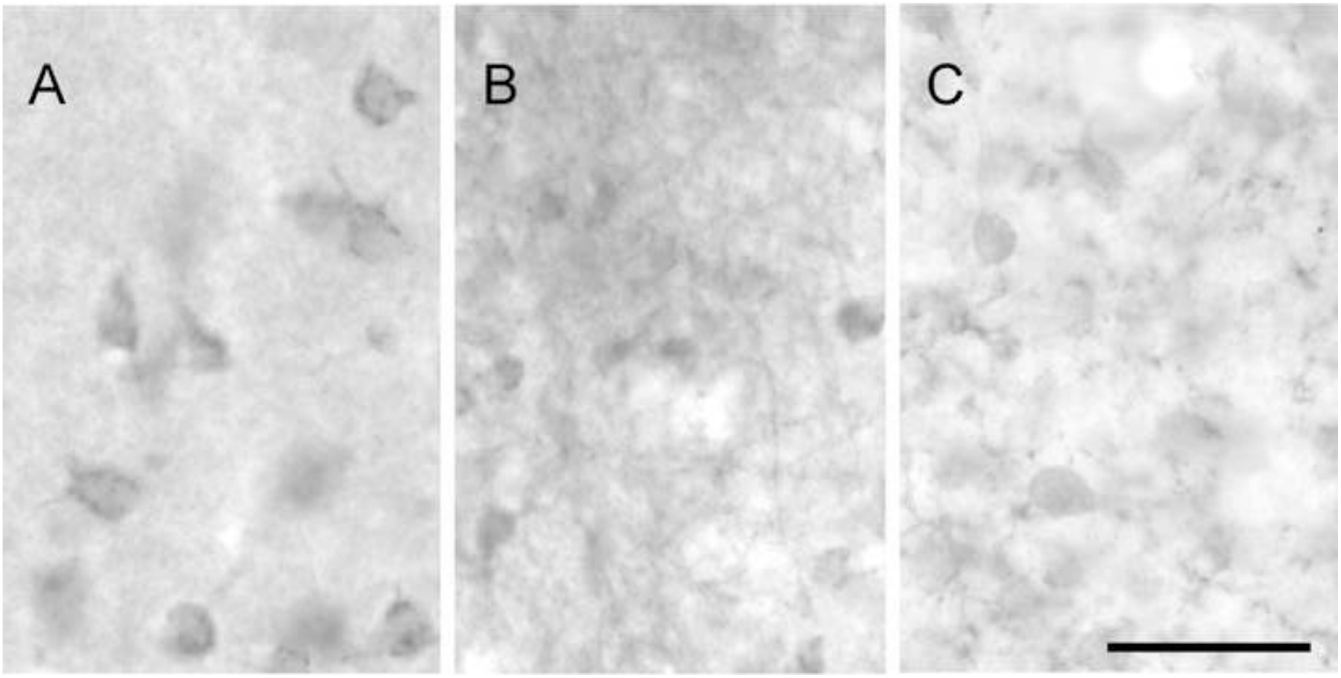

Figure 2.

D1R-labeled processes in the amygdala. **A**: In the BLA, D_1-IR is most intense in a cell bodies in a reticular network that surrounds the nucleus, with weaker somatic and punctate neuropil label seen. **B**: Within the intercalated cell groups, D_1-IR is found in immunoreactive fibers in the neuropil. **C**: In the BLA, D_5-IR is found in both cell bodies and the neuropil where both puncta and processes were labeled. Scale bar is 50 μm.

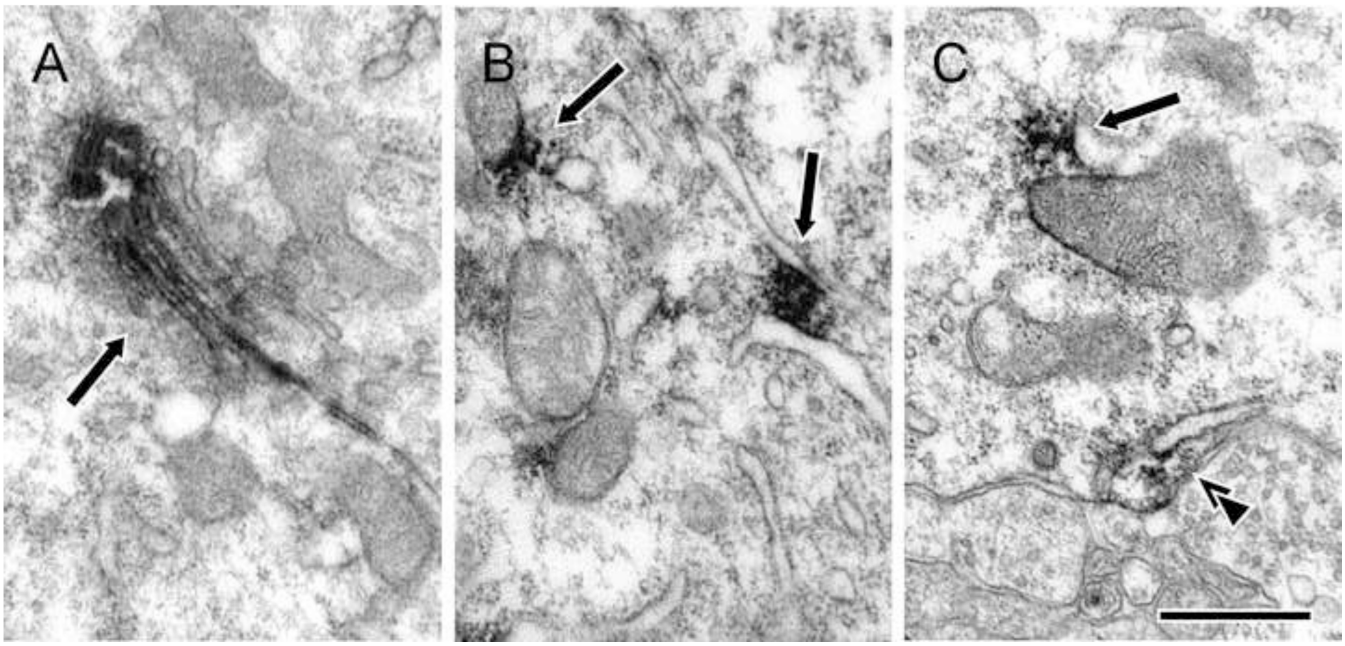

Figure 3.

Electron micrographs illustrating examples of D1R immunoreactivity in BLA cell soma. **A**: D_1-IR (arrows) was observed commonly in the Golgi apparatus of BLA neurons. **B**: D_1-IR was also sometimes seen associated with other internal membranes. **C**: D_5-IR was observed in close proximity to a variety of internal membranes as well as the plama membrane (double arrowhead). Scale bar is 500 nm.

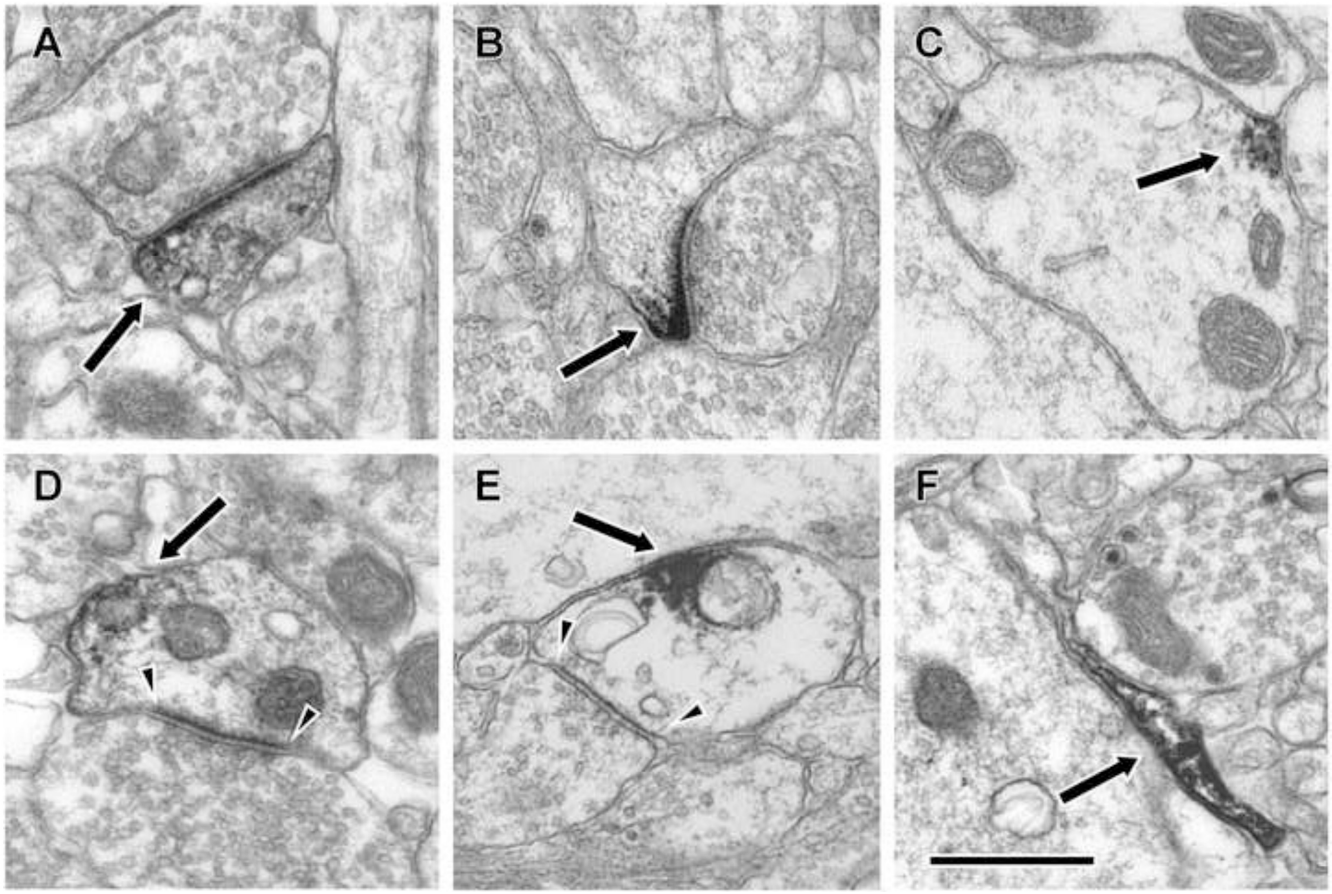

Figure 4.

Electron micrographs illustrating examples of D1R-IR in BLA neuropil. Diaminobenzidine label (arrows) was identified in spines for both D_1 (**A**) and and D_5 (**B**). Examples of dendrites containing D_5-IR (**C**) and D_1-IR (**D, E**) were also frequently identified. These labeled dendrites were sometimes observed to receive asymmetric (arrowheads, **D**) and symmetric (arrowheads, **E**) synaptic contacts. In addition to label in the dendritic arbors of neurons, label was also observed in glial processes as illustrated in **F** for a D_1-IR process. Scale bar is 500 nm.

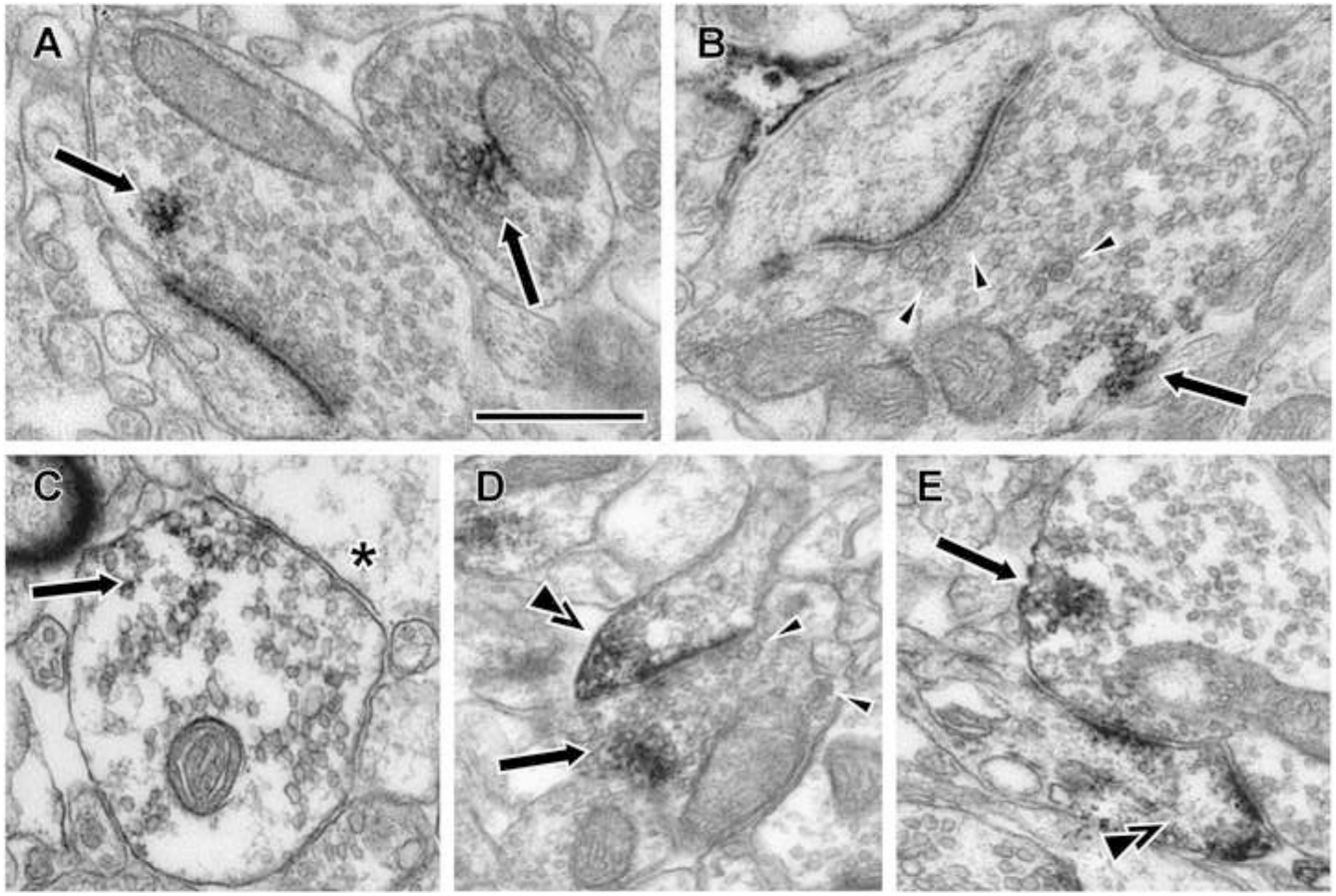

Figure 5.

Electron micrographs illustrating examples of D1R-IR axon terminals in the BLA neuropil. Diaminobenzidine label for D_5 (**A** and **B**) and D_1 (**C, D** and **E**) is indicated by arrows. Labeled axon terminals were observed to make asymmetric (**A** and **B**) and symmetric synaptic contacts (**C**). Note the omega structure in **C** (across from *), indicating a vesicle fusing with the plasma membrane. Some D1R-IR axon terminals contained dense core vesicles (arrow heads, **B** and **D**). In addition, some examples of D_1-IR terminals synapsing onto D_1-IR spines (double arrowheads) were observed (**D** and **E**). Scale bar is 500 nm.

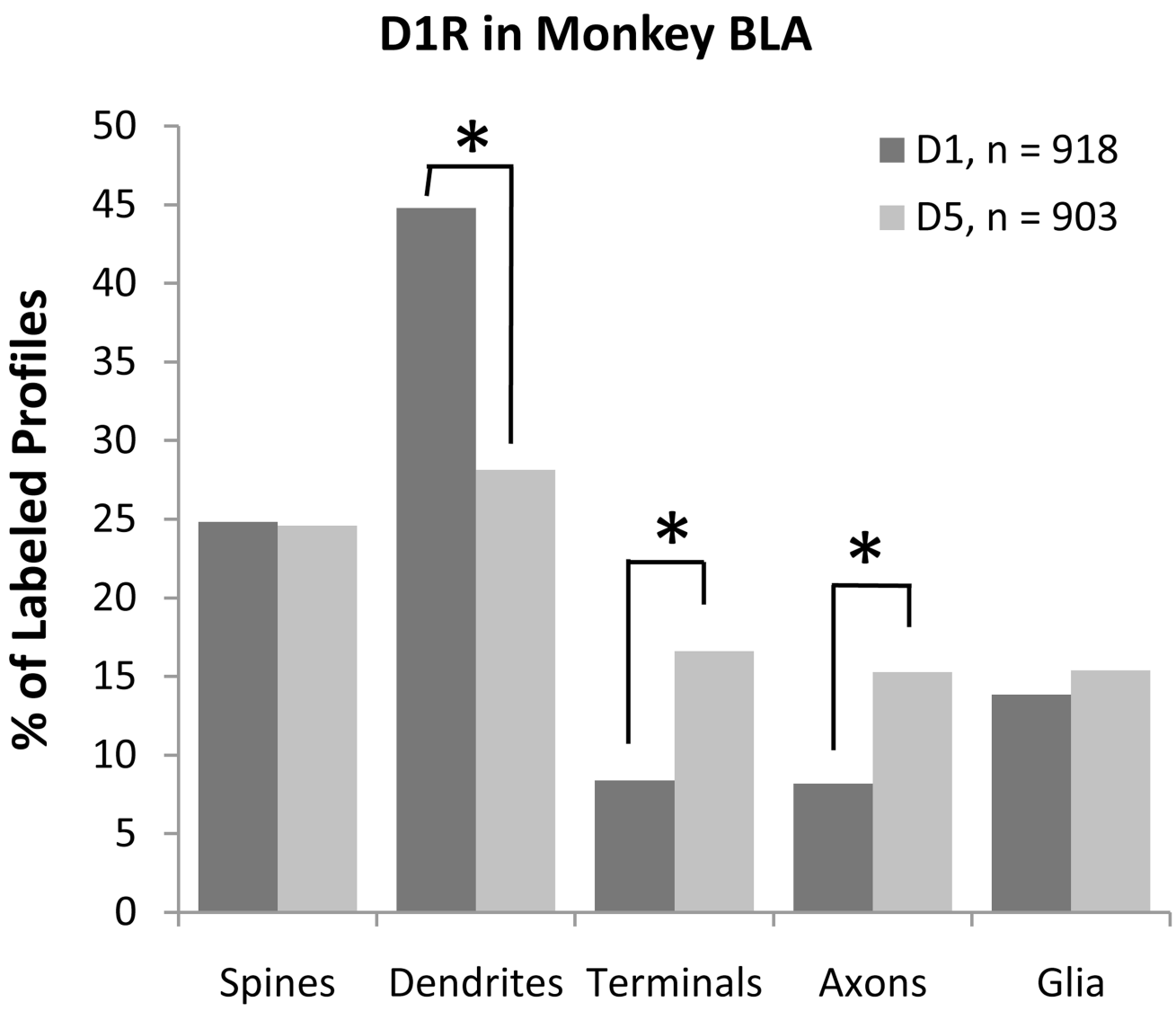

Figure 6.

A histogram comparing the relative abundance of D_1 and D_5 in the BLA of the rhesus monkey. The distribution of D_1 and D_5 differed significantly (χ^2= 79.679; p<0.0001). Post-hoc testing revealed that dendritic shafts were more commonly labeled for D_1, while preterminal axons and axon terminals were more commonly labeled for D_5. Comparisons that are significantly different by post-hoc tests are indicated by an asterisk.

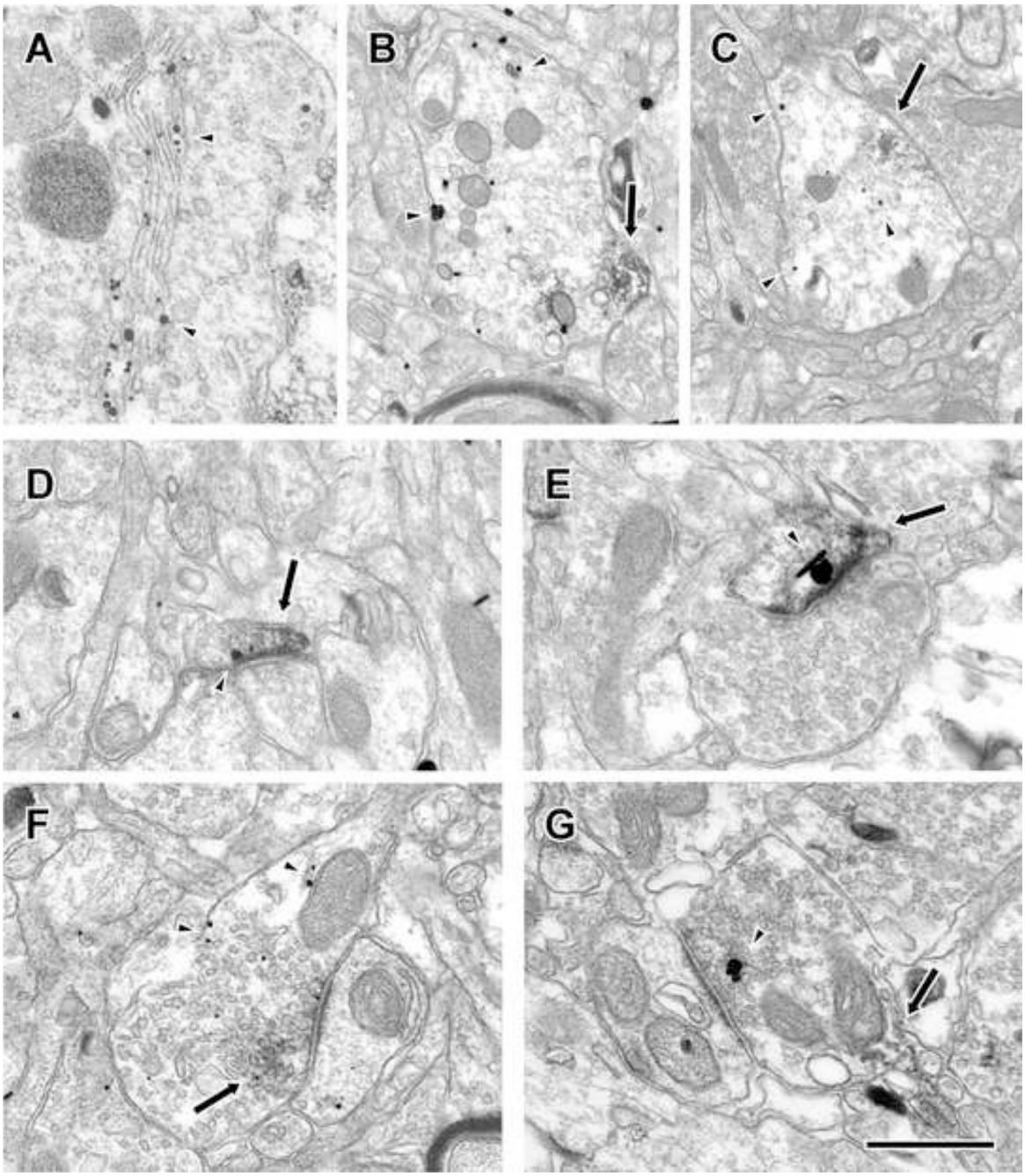

Figure 7.

Electron micrographs of double-label immunogold (arrowheads) and DAB (arrows) images of D_1 and D_5 in PFC. **A:** D_1-gold label in the golgi apparatus of a cell soma. **B, C:** Double-labeled dendrites in which either D_1 (**B**) or D_5 (**C**) is labeled with gold. **D, E:** Double-labeled spines in which either D_1 (**D**) or D_5 (**E**) is labeled with gold. **F, G:** Double-labeled axon terminals in which either D_1 (**F**) or D_5 (**G**) is labeled with gold. Scale bar is 500 nm, except in **B** and **C** where it is 900 nm.

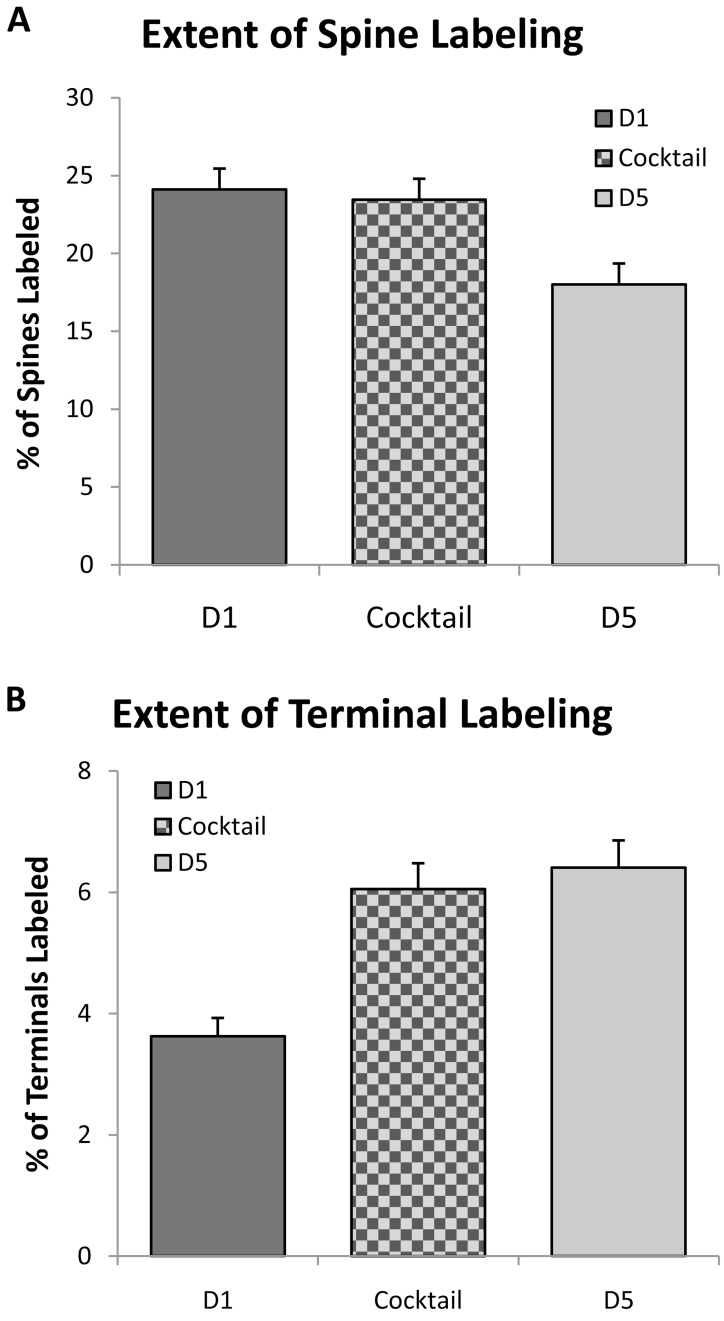

Figure 8.

A: A graph showing the extent to which BLA spines are labeled after immunohistochemistry for D_1, D_5 or a cocktail of the two antibodies. Images from four different animals were examined and spines receiving asymmetric synapses were identified. For each image, the percentage of spines that were immunolabeled was identified and the mean and standard deviation for each condition is graphed. The number of images analyzed was 629 for D_1, 489 for D_5 and 572 for the cocktail. ANOVA and post-hoc Scheffe tests confirmed that the cocktail condition did not label significantly more spines than the D_1 condition alone, indicating that D_5 receptor is found in a subpopulation of spines that also contain the D_1 receptor. **B**: A graph showing the extent to which BLA terminals are labeled after

immunohistochemistry for D_1, D_5 or a cocktail of the two antibodies. Images from four different animals were examined and axon terminals were identified based on their content of synaptic vesicles. For each image, the percentage of terminals that were immunolabeled was identified and the mean and standard deviation for each condition is graphed. The number of images analyzed was 748 for D_1, 606 for D_5 and 670 for the cocktail. ANOVA and post-hoc Scheffe tests confirmed that the cocktail condition did not label significantly more spines than the D_5 condition alone, indicating that D_1 receptor is found in a subpopulation of spines that also contain the D_5 receptor.

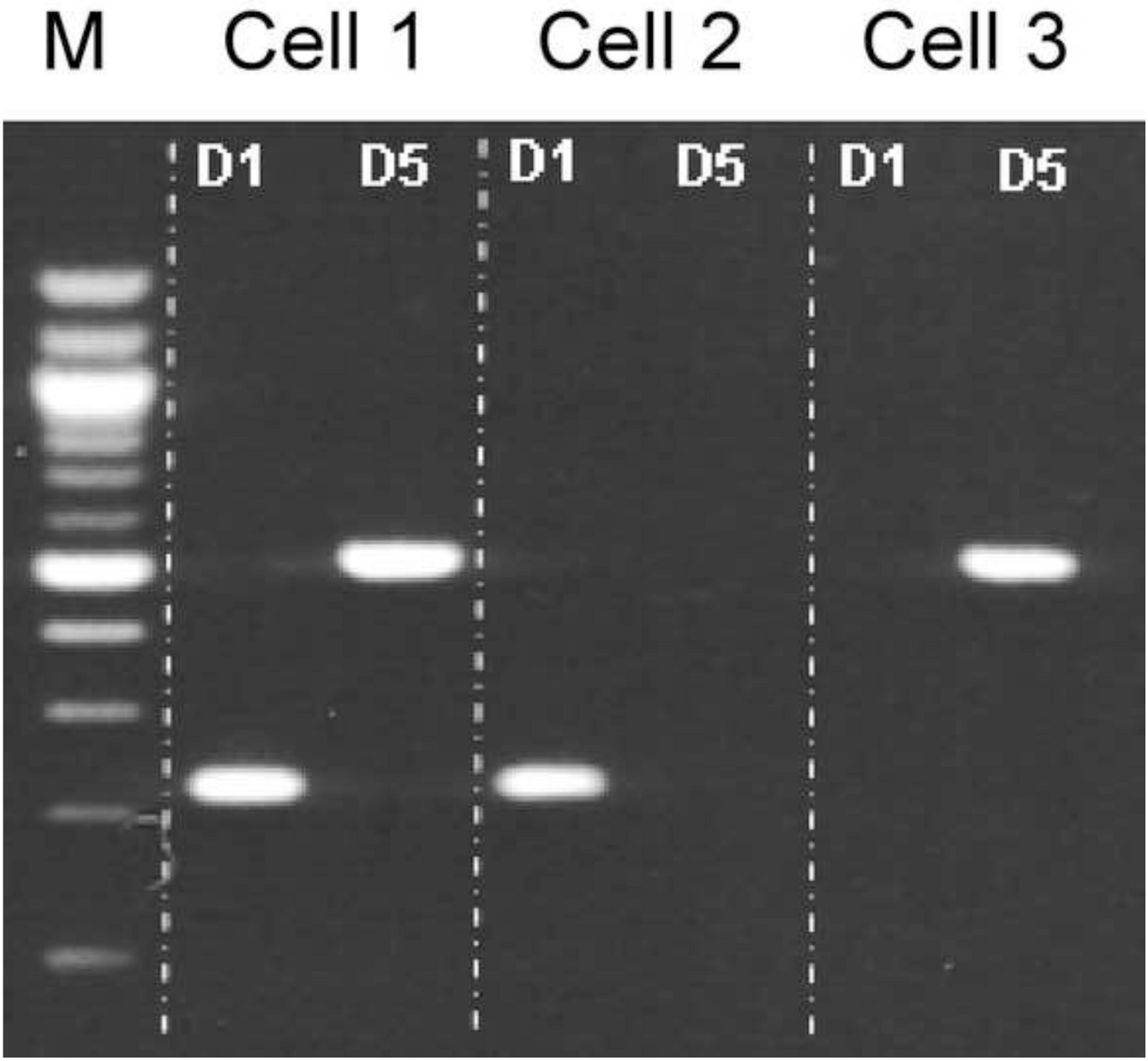

Figure 9.

A photograph of a representative ethidium bromide stained agarose gel in which dopamine receptor D_1 (225 bp) and D_5 (517 bp) mRNA amplicons from single primate BLA projection neurons have been separated by electrophoresis. In Cell 1, both D_1 and D_5 mRNAs were co-expressed. In Cell 2, only the expression of D_1 mRNA could be detected. In Cell 3, D_1 mRNA was not detected while expression of D_5 mRNA was detected. The lane labeled M is a molecular weight marker ladder.

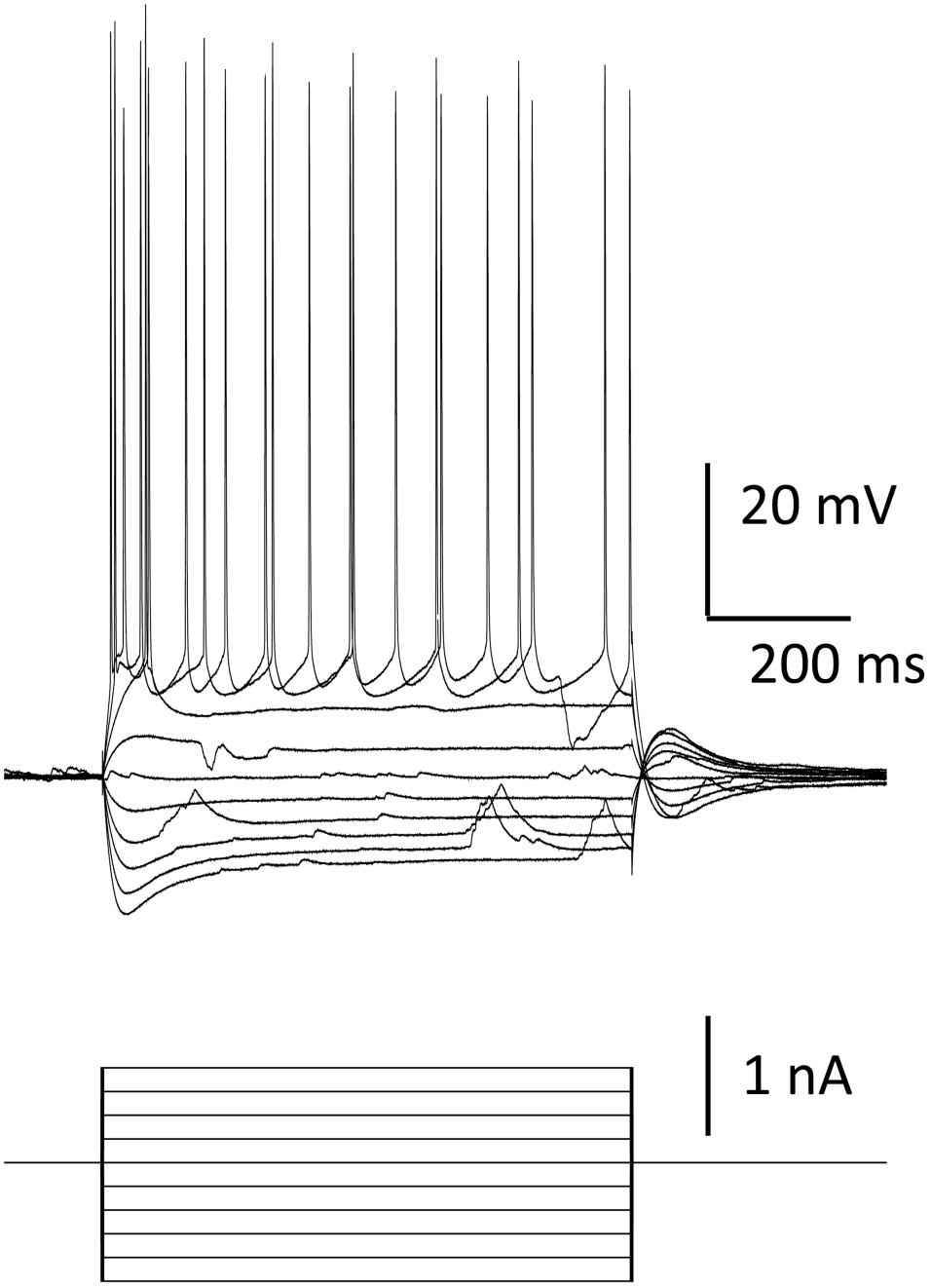

Figure 10.

The prototypical voltage response (upper trace) of a primate BLA projection neuron in response to transient (750 ms) current injection (lower trace). In response to supra-threshold depolarizing current injection most neurons fire a short burst of action potentials and then settle to a rhythmic pattern of action potential generation. In response to hyperpolarizing current injection projection neurons display a prominent depolarizing sag in the membrane voltage response. Note the occurrence of long duration spontaneous inhibitory synaptic potentials (IPSPs) in most of the voltage traces.

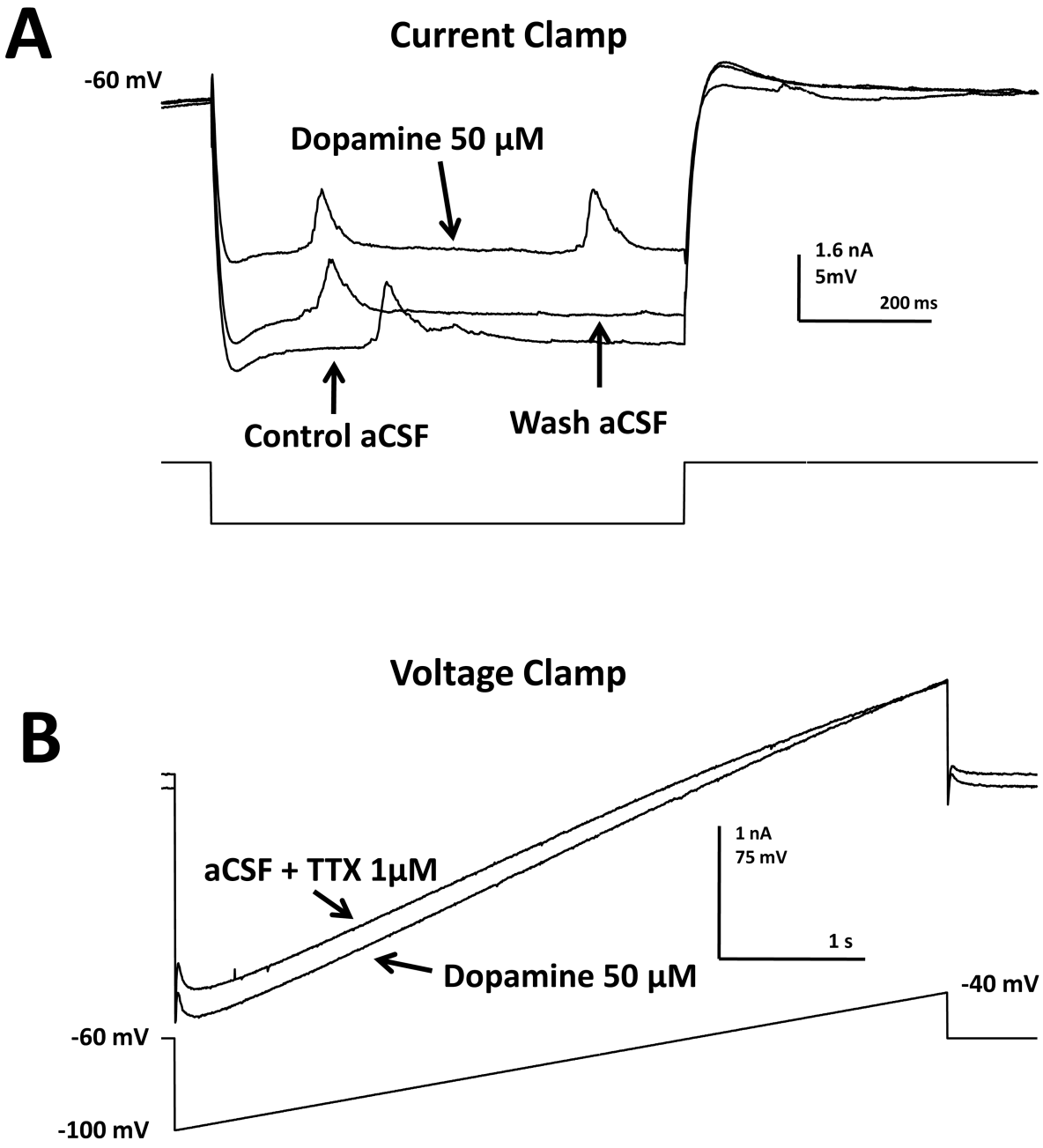

Figure 11.

Dopamine receptor activation in projection neurons of the non-human primate evokes a membrane depolarization that is associated with an increase in membrane conductance. **A:** An overlay of the voltage response (upper traces) to a transient hyperpolarizing current injection (750 ms; 150 pA; lower trace) recorded in a projection neuron of the primate BLA before, during, and after exogenous dopamine (50 µM) application. Note the significant reduction in the amplitude of the voltage response in the presence of dopamine that reverses on washout with aCSF. **B:** In the same neuron, ramping the membrane voltage between −100 and −40 mV before and during dopamine (50 µM) application revealed dopamine-

induced inward current (105 pA) that was associated with an increase in membrane conductance and which had an apparent reversal potential of −42 mV.

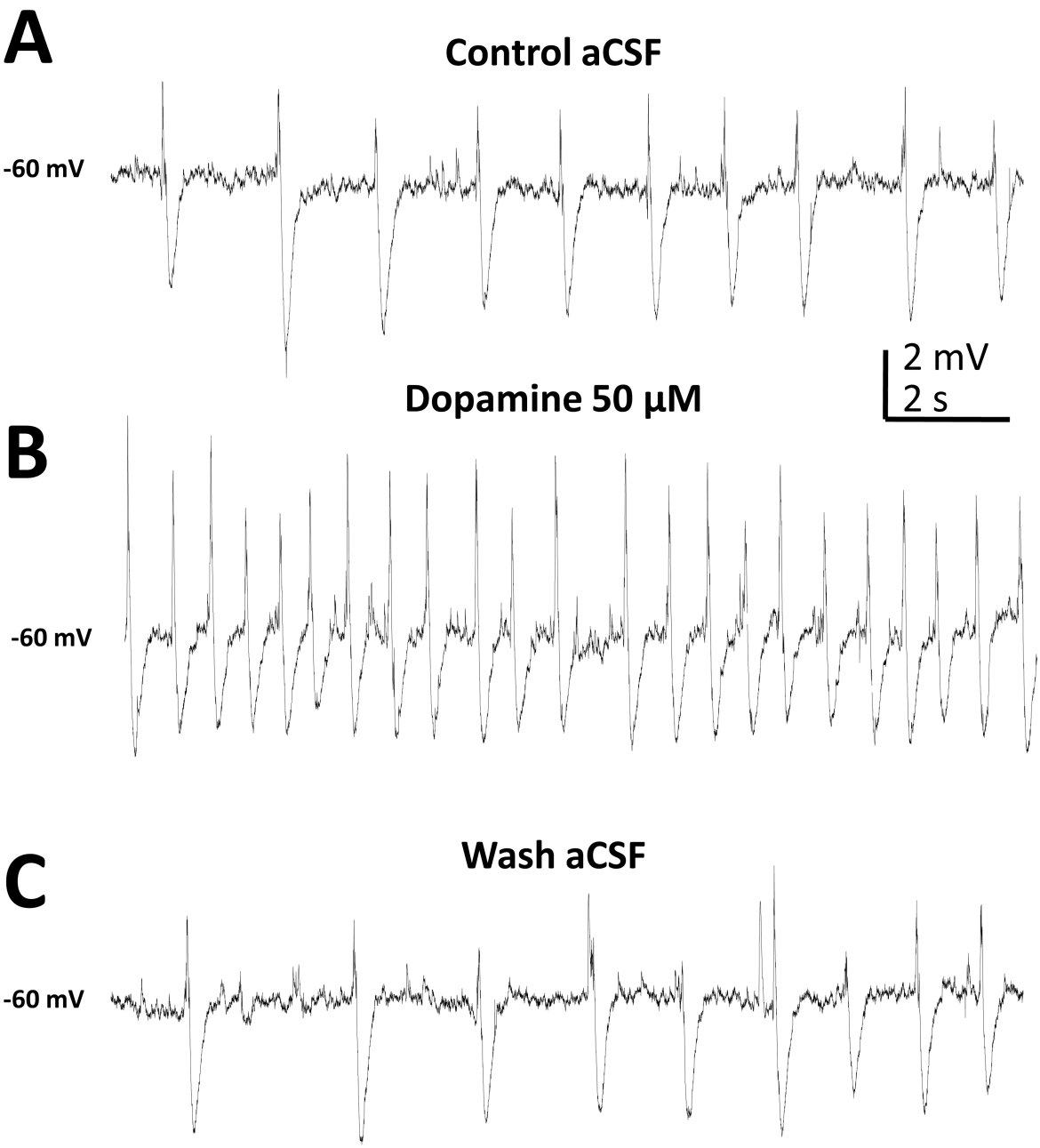

Figure 12.
Dopamine increases the frequency of spontaneous IPSPs in BLA projection neurons. **A:** A voltage trace showing the presence of long duration rhythmic IPSPs at the resting membrane potential of this neuron. **B:** In the same neuron application of dopamine (50 µM) significantly increased the frequency of spontaneous IPSPs. **C:** IPSP frequency returned to pre-drug levels on washout.

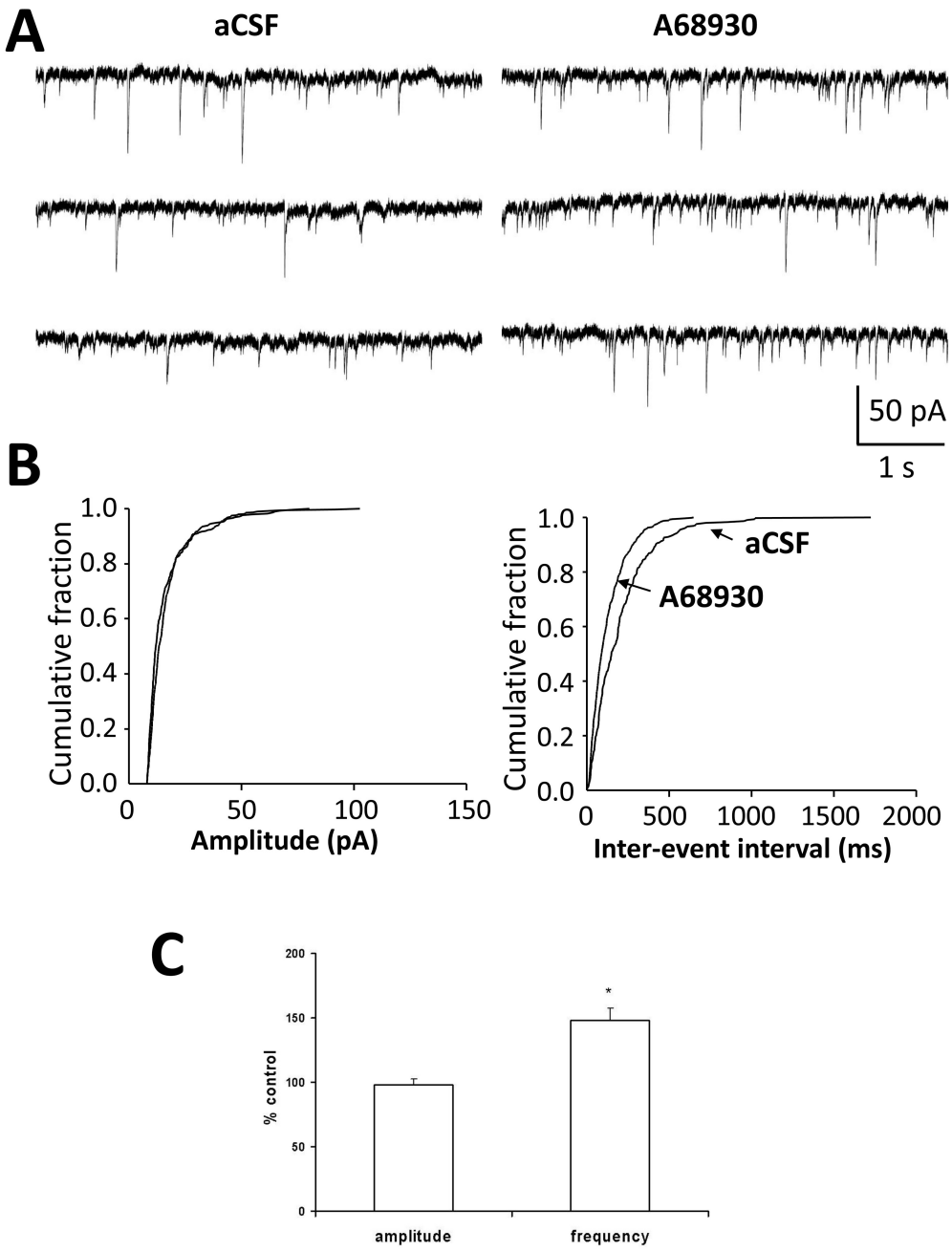

Figure 13.

Dopamine acts at presynaptic D1 receptors to facilitate glutamate release in primate BLA. **A:** Spontaneous miniature excitatory postsynaptic currents (mEPCs) recorded from a BLA projection neuron in the presence of tetrodotoxin (TTX, 1 μM; left traces) increase in frequency in the presence of the D1 receptor agonist A68930 (50 μM; right traces). **B:** Cumulative fraction plots showing that application of the D1 selective agonist A68930 increases the frequency (right plot) but not the amplitude (left plot) of mEPSCs. **C:** A histogram showing the relative increase in mEPSC amplitude following application of A68930 by treatment group (n=6; * = $p < 0.05$).

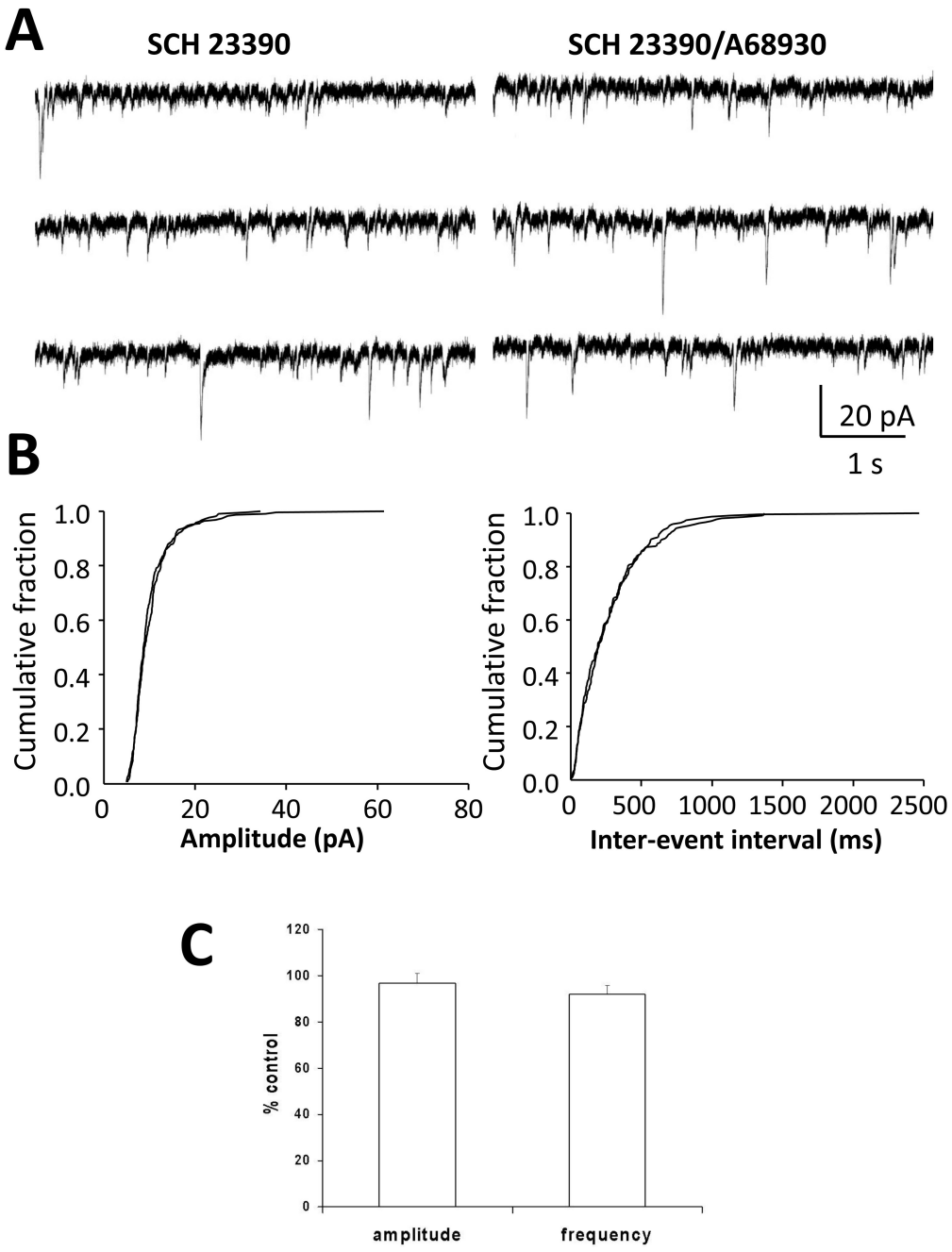

Figure 14.

Prior application of the selective D1R antagonist, SCH 23390, blocked the D1R agonist-induced facilitation of presynaptic glutamate release. **A:** Application of SCH 23390 (20 μM; left traces) had no effect on the frequency or amplitude of spontaneous mEPSCs, but fully blocked the increased mEPSC frequency observed in the presence of the D1 receptor agonist (A68930, 50 μM; right traces). **B:** Cumulative fraction plots showing that application of A68930 (50 μM) has no effect on either the amplitude (left plot) or the frequency (right plot) of mEPSCs in the presence of the D1 receptor selective antagonist SCH 23390. **C:** A histogram showing the group data for the SCH 23390 blockade of the A68930-induced increase in mEPSC frequency (n=6).

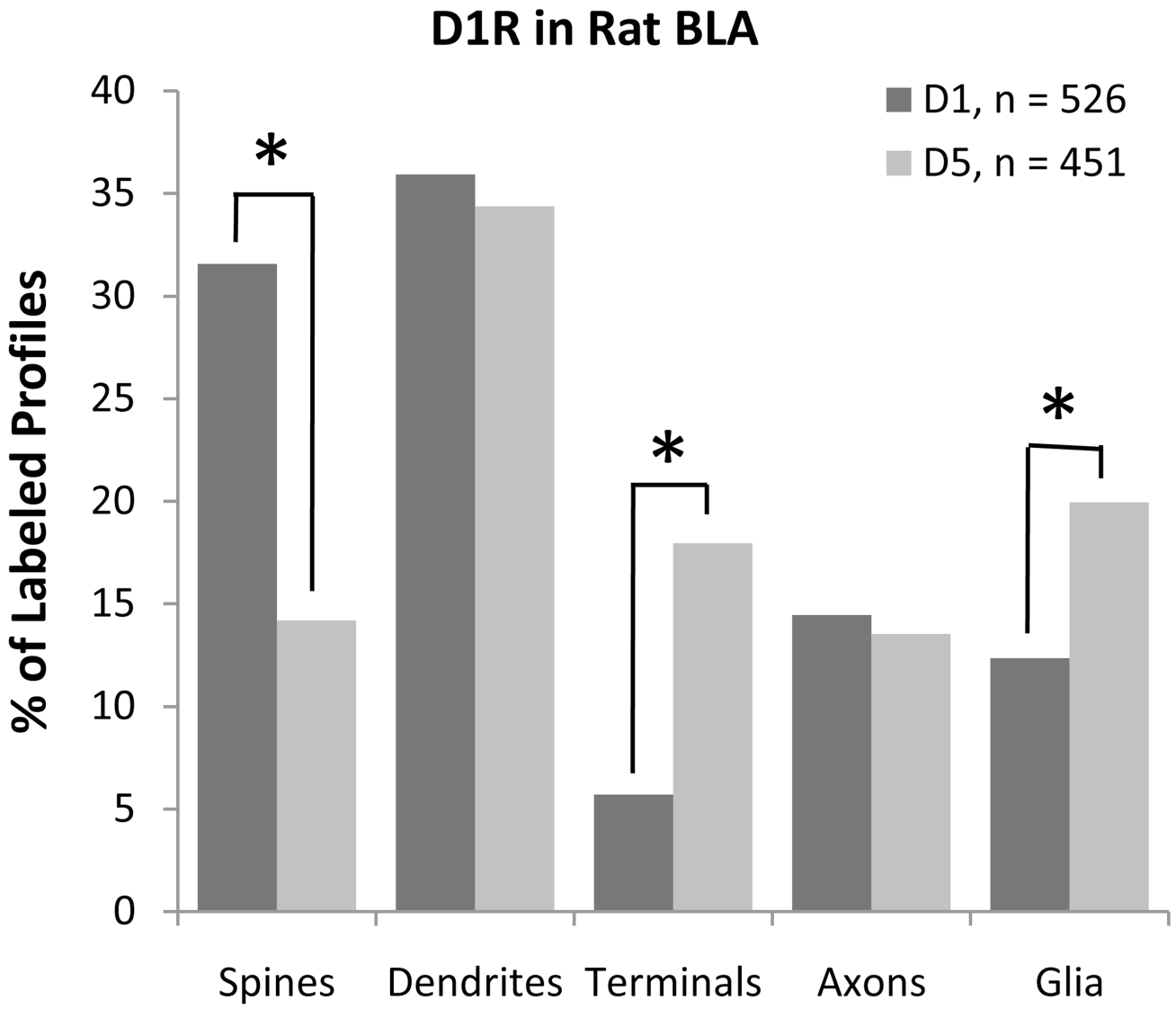

Figure 15.

A histogram comparing the relative abundance of D_1 and D_5 in the BLA of the rat. The distribution of D_1 and D_5 differed significantly (χ^2= 2.371; p<0.0001). Post-hoc testing revealed that dendritic spines were more commonly labeled for D_1, while axon terminals glia were more commonly labeled for D_5. Comparisons that are significantly different by post-hoc tests are indicated by an asterisk.

Table 1

A comparative analysis of some basic membrane properties of BLA projection neurons of the rat and primate.

Primate Projection Neuron Basic Cell Properties							
RMP (mV)	**Rm (mΩ)**	**Tau (ms)**	**Threshold (mV)**	**Amplitude (mV)**	**Half Width (ms)**	**Rise Time (ms)**	**Decay Time (ms)**
−64.4±0.5	39.0±5.5 #	20.6±1.8	−47.2±1.0	89.3±1.2	1.1±0.1 #	0.4±0.1	1.5±0.1 #
N=12	N=12	N=12	N=12	N=12	N=12	N=12	N=12
Rat Projection Neuron Basic Cell Properties							
−60.5±0.3	71.1±3.6	21.1±1.3	−44.61±0.7	85.6±2.3	0.89±0.1	0.36±0.1	0.92±0.1
N=20	N=20	N=20	N=20	N=20	N=20	N=20	N=20

# Denotes significance at $p < 0.05$.